



Escuer, J., Cebollero, M., Peña, E., McGinty, S. and Martinez, M. A. (2020) How does stent expansion alter drug transport properties of the arterial wall? *Journal of the Mechanical Behavior of Biomedical Materials*, 104, 103610. (doi: [10.1016/j.jmbbm.2019.103610](https://doi.org/10.1016/j.jmbbm.2019.103610))

The material cannot be used for any other purpose without further permission of the publisher and is for private use only.

There may be differences between this version and the published version. You are advised to consult the publisher's version if you wish to cite from it.

<http://eprints.gla.ac.uk/207345/>

Deposited on 06 January 2020

Enlighten – Research publications by members of the University of  
Glasgow

<http://eprints.gla.ac.uk>

# How Does Stent Expansion Alter Drug Transport Properties of the Arterial Wall?

Javier Escuer<sup>a</sup> Martina Cebollero<sup>a</sup> Estefanía Peña<sup>a,b</sup> Sean McGinty<sup>c</sup>  
Miguel A. Martínez<sup>a,b,\*</sup>

<sup>a</sup>*Aragón Institute for Engineering Research (I3A), University of Zaragoza, Spain*

<sup>b</sup>*Biomedical Research Networking Center in Bioengineering, Biomaterials and Nanomedicine (CIBER-BBN), Spain.*

<sup>c</sup>*Division of Biomedical Engineering, University of Glasgow, Glasgow, UK*

---

## Abstract

Stents have become the most successful device to treat advanced atherosclerotic lesions. However, one of the main issues with these interventions is the development of restenosis. The coating of stents with antiproliferative substances to reduce this effect is now standard, although such drugs can also delay re-endothelialization of the intima. The drug release strategy is therefore a key determinant of drug-eluting stent efficacy. Many mathematical models describing drug transport in arteries have developed and, usually separately, models describing the mechanics of arterial tissue have been devised. However, there the literature is lacking a comprehensive model that adequately takes into account both the mechanical deformation of the porous arterial wall and the resulting impact on drug transport properties. In this paper, we provide the most comprehensive study to date of the effect of stent mechanical expansion on the drug transport properties of a three-layer arterial wall. Our model incorporates the state-of-the-art description of the mechanical properties of arterial tissue through an anisotropic, hyperelastic material model and includes a nonlinear saturable binding model to describe drug transport in the arterial wall. We establish relationships between mechanical force generated through device expansion and alteration in diffusion within the arterial wall and perform simulations to elucidate the impact of such alterations in spatio-temporal drug release and tissue uptake. Mechanical deformation of the arterial wall results in modified drug transport properties and tissue drug concentrations, highlighting the importance of coupling solid mechanics with drug transport.

*Key words:* Drug-eluting stent, Mechanical expansion, Drug transport, Arterial wall, Coupling mechanics-drug transport, Anisotropic hyperelastic material

---

\* Corresponding author. Miguel A. Martínez. Mechanical Engineering Department. c/ María de Luna s/n 50018. Zaragoza. Spain. Tel.: +34 87655252; Fax: +34 976762578  
*Email address:* miguelam@unizar.es (Miguel A. Martínez).

## 1 Introduction

Coronary heart disease (CHD) is the leading cause of death worldwide [1]. CHD is attributed to atherosclerosis, the hardening and narrowing of the arterial lumen due to the build-up of cholesterol and fatty deposits on the inner wall of the vessel. This in turn reduces blood flow through the coronary arteries to the heart muscle.

Stent implantation has become the most successful strategy in the treatment of CHD by percutaneous coronary intervention (PCI). However, in-stent restenosis (ISR), a gradual luminal re-narrowing mainly due to the vessel wall injury induced by the device, is the major clinical limitation of this technique [2]. The introduction of drug-eluting stents (DES), which release antiproliferative substances into the arterial tissue has contributed to the dramatic reduction in incidence of ISR to less than 10% [3]. However, the risk of developing late or very-late stent thrombosis (ST) is typically higher with the use of DES compared with bare-metal stents, and given the high mortality rates associated with ST, this issue remains an important safety concern that needs to be addressed [2, 4].

The use of computational (*in silico*) modelling and simulation for coronary stents has emerged as a powerful technique that can contribute to addressing some of the limitations of often difficult and expensive experimental analysis [5, 6]. In terms of simulating the deployment of a stent inside a coronary artery, these models can provide useful insights into the stress-strain response that the device induces within the arterial tissue and how stent design factors contribute to mechanical performance *in vivo*. In the literature, several *in silico* studies with different levels of complexity have been performed to investigate geometrical and material properties of stents, different deployment strategies, effects of arterial curvature, the use of patient-specific geometries and the inclusion of stenosis and atherosclerotic tissue [5, 7–12]. However, these models do not adequately account for drug-transfer from a DES.

In the context of drug transport modelling, computational analysis can contribute to a better understanding of drug-release and binding mechanisms in arteries, aiming to guide the development of a next generation of DES with more favourable safety and efficacy [13]. A large number of computational studies have been developed in the last decade for this purpose, adopting either well-defined one-dimensional simplifications [6, 14–20], or two-dimensional [21–31] and three-dimensional formulations [32–35]. These models generally consider an intact vessel with diffusion, advection and binding dictating the transport of drugs within the blood flow and the respective wall layers. However, these models do not take account of the influence of mechanical deformation on drug transport. In terms of modelling the drug binding process in the arterial wall, a nonlinear saturable reversible binding model is currently the well-accepted approach [15, 25, 28]. The precise form of modelling binding is controversial, however, with some authors highlighting the importance of taking into account binding to specific receptors and binding to non-specific sites (general extracellular matrix sites) as two separate phases [6, 36]. In terms of modelling drug dynamics within the stent coating, although most models assume that drug transport is governed purely by diffusion [24, 25, 28], depending on the physical and chemical characteristics of the polymeric coating and of the drug, it may be necessary to also account for other phenomena such as dissolution [6, 19], degradation [29, 31, 37] or erosion [37].

There are a limited number of studies that attempt to incorporate both the mechanics of arterial tissue and drug transport. For example, in their 3D models, Migliavacca et al. [32] and Cutrì et al. [35] include drug transport in an arterial wall deformed by their simulations of stent deployment, but neither model relates the drug transport parameters to the level of deformation. Ferreira et al. [29, 31] use a linear viscoelastic model to explore how drug diffusion may be hindered in the presence of atherosclerotic plaque, but do not account for mechanical deformation of the arterial wall as a result of stent deployment. Feenstra and Taylor [34], through a porohyperelastic-transport approach, calculate the geometry, porosity field and interstitial fluid velocity directly from a simulation of stent deployment and use these within a model of drug transport in the arterial wall consisting of three distinct layers. In this sense, tissue porosity and the contribution to drug transport of advection are not assumed *a priori*. However, this model assumes a linear drug reaction and drug diffusion coefficients that do not vary with deformation. Denny et al. [26, 27] do model the influence of strut compression on local diffusivity [26, 27] through simulations of the compression of an idealised arterial wall by an idealised unit cell model of a stent, but their model does not adequately account for the effects of nonlinear binding of drug.

In this paper, we provide the most comprehensive study to date of the effect of stent mechanical expansion on the drug transport properties of a three-layer arterial wall. Our model incorporates the state-of-the-art description of the mechanical properties of arterial tissue through an anisotropic, hyperelastic material model and includes a nonlinear saturable binding model to describe drug transport in the arterial wall. We establish relationships between mechanical force generated through device expansion and alteration in diffusion within the arterial wall and perform simulations to elucidate the impact of such alterations in spatio-temporal drug release and tissue uptake.

## 1.1 Outline

We start with a discussion of the mechanical aspect of the problem and present the material models employed to describe the stent-induced deformation of arterial tissue. We then derive expressions for the arterial drug diffusion coefficients as a function of deformation (Section 2.2). This is followed by a description of the drug transport model in the lumen, where blood flow is described by the steady Navier-Stokes equations, and in the multi-layer anisotropic porous tissue of the arterial wall, where Darcy's law is used to calculate the plasma filtration through the tissue and advection-diffusion-reaction equations are used to model the drug dynamics (Section 2.3). A detailed description of the computational geometry and the implementation of the model equations is provided in Section 2.4. The key results are presented in Section 3, along with a discussion of their significance. Finally, in Section 4 and 5 we reiterate the limitations of our work and provide some final conclusions, respectively.

## 2 Material and Methods

### 2.1 Mechanical model

#### 2.1.1 Modelling the arterial wall

We consider the arterial wall to be composed of three distinct layers: the intima, the media and the adventitia. Each individual layer is modelled as an anisotropic, hyperelastic and incompressible material [38, 39] and reinforced by two families of collagen fibres, following the model proposed by Gasser et al. [40]. In this model, the strain-energy function (SEF) is given by:

$$\Psi = \mu (I_1 - 3) + \sum_{\alpha=4,6} \frac{k_1}{2k_2} \left[ \exp \left\{ k_2 [\kappa I_1 + (1 - 3\kappa)I_\alpha - 1]^2 \right\} - 1 \right], \quad (1)$$

where  $I_1 = \text{tr}(\mathbf{C})$  represents the first invariant of the right Cauchy-Green deformation tensor [41],  $\mathbf{C}$ , characterizing the isotropic mechanical response of the elastin [42, 43] while  $I_4 \geq 1$  and  $I_6 \geq 1$  characterize the mechanical response in the preferential directions of the fibers/cells [39]. The material parameters  $\mu > 0$  and  $k_1 > 0$  have the dimension of stress whereas  $k_2 > 0$  and  $0 \leq \kappa \leq 1/3$ , that characterizes the level of dispersion of the collagen orientations, are dimensionless. When  $\kappa = 0$  the fibres are perfectly aligned (no dispersion) and when  $\kappa = 1/3$  the fibres are randomly distributed and the material becomes isotropic. Assuming that the anisotropy directions are helically oriented at  $\pm\beta$  degrees with respect to the longitudinal direction, the invariants  $I_4$  and  $I_6$  can also be expressed as a function of the main stretches:

$$I_4 = \lambda_1^2 \cos^2 \beta_1 + \lambda_2^2 \sin^2 \beta_1, \quad I_6 = \lambda_1^2 \cos^2 \beta_2 + \lambda_2^2 \sin^2 \beta_2. \quad (2)$$

where  $\beta_1 = \beta$  and  $\beta_2 = -\beta$  [44]. Moreover, it has been assumed that the strain energy corresponding to the anisotropic terms only contributes to the global mechanical response of the tissue when stretched, that is  $I_4 > 1$  and  $I_6 > 1$ , and that the tissue does not bear any load when compressed. The model parameters were calibrated against the experimental data reported by Holzapfel et al. [39] and shown in Table 1. Notice that all tissues have been considered as incompressible for this material parameter identification, i.e. with volume ratio  $J = \det \mathbf{F} = 1$ , where  $\mathbf{F}$  is the deformation gradient tensor.

#### 2.1.2 Modelling stent struts and stent coating

The stent struts are modelled as an elasto-plastic material with a Young's modulus,  $E$ , of 200 GPa and Poisson's ratio,  $\nu$ , of 0.28, representative of biomedical grade stainless steel alloy 316L [5]. The plasticity is described by isotropic hardening  $J_2$  flow theory with the tensile stress-strain curves taken from the literature [45], including a yield strength,  $\sigma_y$ , of 264 MPa and a ultimate tensile strength

(UTS),  $\sigma_u$ , of 584 MPa at an engineering plastic strain of 0.247. The stent coating is modelled as a nonlinear elastic material with bilinear behaviour simulating a phosphorylcholine (PC)-based polymer coating with a Young's modulus of 240 MPa, a Poisson's ratio of 0.5, a yield strength of 16 MPa and a tangent modulus,  $E_t$ , of 7.7 MPa [46,47].

[Table 1 about here.]

## 2.2 Derivation of arterial diffusion coefficients as a function of deformation

In a porous media, as in the case of the arterial wall, diffusion of species takes place over a tortuous path that depends on the material structure [48]. The influence of the porosity coupled with the tortuous nature of the arterial tissue results in the so-called effective diffusivity or effective diffusion coefficient,  $D$ , which is defined as [49]:

$$D = \frac{\phi}{\tau} D_{free}, \quad (3)$$

where  $\phi$  is the porosity,  $\tau$  represents the tortuosity and  $D_{free}$  is the species free diffusivity which is determined by the Stokes-Einstein equation [49]:

$$D_{free} = \frac{k_B T}{6\pi\mu R}, \quad (4)$$

where  $T$  is the absolute temperature,  $k_B$  is the Boltzmann's constant,  $\mu$  is the dynamic viscosity of the solvent (plasma) and  $R$  is the hydrodynamic solute (drug) radius. Due to the heterogeneous structure of the arterial wall, the effective diffusion coefficient will be different for each layer of the tissue [50]. Moreover, there is experimental evidence to suggest that diffusion within each layer is anisotropic [51,52]. Tortuosity can be estimated by the ratio between the average pore path length,  $L$ , to the straight distance between the ends of the pore path,  $X$ , as:  $\tau = L/X$  [50]. Although the pore pathways in the arterial tissue runs through different 3D planes, since we consider a 2D axisymmetric model in this work, we consider diffusion in the radial and longitudinal directions only. It is assumed that after stent implantation the arterial wall is radially compressed by the stent struts, leading to changes in tortuosity, and therefore in arterial diffusivity, in both radial and longitudinal directions [27, 53]. Fig. 1 shows how stenting theoretically affects the tortuous path in both directions. The stent expansion will also cause local changes to porosity in the arterial tissue. However, these local variations are not taken into account in the analysis framework presented assuming that the overall porosity in each layer is constant. In the radial direction, a variation in the thickness of each layer of the arterial wall ( $X_i$ ) is observed, resulting in an increase in tortuosity in that direction:

$$\tau_{i,r} = \frac{L_{i,r}}{X_i + \Delta X_i}, \quad (5)$$

where the subscript  $i = \{ses, m, a\}$  denotes the subendothelial space of the intima, the media and the adventitia, respectively; the subscript  $r$  denotes the radial direction;  $L_{i,r}$  is the length of the pore path in each layer, which is assumed to remain constant [50] and;  $\Delta X_i$  represents the change in each wall layer thickness and is positive for an increase but negative for a decrease in thickness. The definition of radial strain,  $\varepsilon_{i,r} = \Delta X_i / X_i$ , is used to relate the tortuosity after compression in the radial direction in each layer of the tissue,  $\tau_{i,r}$ , to the uncompressed wall tortuosity,  $\tau_{i,r}^0$ , as follows:

$$\frac{\tau_{i,r}^0}{\tau_{i,r}} = \frac{L_{i,r}/X_i}{L_{i,r}/(X_i + \Delta X_i)} = 1 + \varepsilon_{i,r}, \quad (6)$$

By relating Eqs. (3) and (6), we can establish a ratio between the initial effective diffusion coefficient,  $D_{i,r}^0$ , and the effective diffusivity after compression,  $D_{i,r}$ , in radial direction:

$$\frac{D_{i,r}^0}{D_{i,r}} = \frac{1}{1 + \varepsilon_{i,r}}. \quad (7)$$

Following the same reasoning, we can obtain a relationship between the initial effective diffusivity in the uncompressed wall longitudinal direction,  $D_{i,z}^0$ , and the effective diffusivity after compression in that direction,  $D_{i,z}$ , through the longitudinal strain,  $\varepsilon_{i,z}$ , and finally define an anisotropic diffusion tensor after stenting for each layer of the tissue,  $\mathbf{D}_i$ , as:

$$\mathbf{D}_i = \begin{pmatrix} D_{i,r} & 0 \\ 0 & D_{i,z} \end{pmatrix} = \begin{pmatrix} D_{i,r}^0(1 + \varepsilon_{i,r}) & 0 \\ 0 & D_{i,z}^0(1 + \varepsilon_{i,z}) \end{pmatrix}, \quad (8)$$

where the subscript  $z$  refers to the longitudinal direction. Due to stenting, the arterial wall experiences compressive strain ( $\varepsilon_{i,r} < 0$ ) in the radial direction and tensile strain ( $\varepsilon_{i,z} > 0$ ) in the longitudinal direction, therefore, Eq. (8) shows that the magnitude of the effective diffusivity in the tissue after stent deployment is lower than the uncompressed value in the radial direction and higher than the uncompressed value in the longitudinal one. This assumption is in agreement with the experimental data reported in Levin et al. [52], where it is shown that the radial diffusivity of paclitaxel and sirolimus in the arterial wall in the radial direction is lower than in circumferential and longitudinal directions.

[Fig. 1 about here.]

## 2.3 Drug transport model

### 2.3.1 Modelling blood flow

The blood flow is modelled as a Newtonian fluid and assumed to be steady, laminar and incompressible, described by the stationary Navier-Stokes equations and the continuity equation:

$$\rho_b(\mathbf{u}_l \cdot \nabla)\mathbf{u}_l = -\nabla p_l + \mu_b \nabla^2 \mathbf{u}_l, \quad (9)$$

$$\nabla \cdot \mathbf{u}_l = 0, \quad (10)$$

where  $\mathbf{u}_l$  is the lumen velocity vector,  $p_l$  is the pressure in the lumen,  $\mu_b$  is the blood dynamic viscosity and  $\rho_b$  is the blood density. A laminar Poiseuille velocity profile is imposed at the inlet of the arterial lumen,  $\Gamma_{l,inlet}$ :

$$w_{l,inlet} = 2u_0 \left(1 - \left(\frac{r}{r_l}\right)^2\right), \quad (11)$$

where  $w_{l,inlet}$  denotes the longitudinal component of the blood velocity in the lumen at the inlet,  $u_0$  is the mean blood velocity computed considering a Reynolds number of  $Re_l = 400$  [54],  $r_l$  is the internal radius of the artery at the inlet (unstented region) and  $r$  is the radial coordinate. At the outlet of the lumen,  $\Gamma_{l,outlet}$ , a pressure value of 100 mmHg (13.3 kPa) is fixed [55]. Moreover, a no-slip boundary condition ( $w_l = 0$ ) was considered at the lumen-arterial wall interface,  $\Gamma_{et}$ . In this work, the pulsatile nature of the blood flow is neglected in agreement with previous models [22–25].

### 2.3.2 Modelling the porous media

The coronary artery wall consists of three porous layers and the transmural velocity vector field in each layer,  $\mathbf{u}_i$ , is computed by Darcy's law, constrained with the solenoidal condition on  $\mathbf{u}_i$  arising from the mass conservation law for an incompressible flow [24, 32]:

$$\mathbf{u}_i = \frac{\kappa_i}{\mu_p} \nabla p_i, \quad \nabla \cdot \mathbf{u}_i = 0 \quad (12)$$

where the subscript  $i = \{ses, m, a\}$  denotes the subendothelial space of the intima, the media or the adventitia, respectively;  $\kappa_i$  is the Darcian permeability of each layer of the arterial wall;  $\mu_p$  is the dynamic viscosity of the blood plasma and;  $p_i$  is the pressure within each layer of the tissue. Finally, to mathematically model the fluid volume flux,  $J_v$ , across the semipermeable membranes between layers, we used the well-known Kedem-Katchalsky equations [56]:

$$J_{v,j} = L_{p,j}(\Delta p_j - s_{d,j} \Delta \pi_j), \quad (13)$$

where the subscript  $j = \{et, iel, eel\}$  denotes the endothelium, the internal or the external elastic lamina, respectively;  $L_{p,j}$  is the hydraulic conductivity of each membrane considered;  $\Delta p_j$  is the pressure difference across the semipermeable membrane;  $s_{d,j}$  is the Staverman osmotic reflection coefficient and;  $\Delta \pi_j$  is the osmotic pressure differential across the membranes. Neglecting the contribution due

to osmosis [25, 54], we can formulate the flux  $J_v$  for each membrane considered:

$$J_{v,et} = L_{p,et}\Delta p_{et} = L_{p,et}(p_l - p_{ses}), \quad (14)$$

$$J_{v,iel} = L_{p,iel}\Delta p_{iel} = L_{p,iel}(p_{ses} - p_m) \quad (15)$$

and

$$J_{v,eel} = L_{p,eel}\Delta p_{eel} = L_{p,eel}(p_m - p_a). \quad (16)$$

In this work, it is assumed that the endothelium is completely denuded due to stent placement in regions between struts and upstream and downstream of the stent over a distance that is one half of the interstrut spacing, measured from the stent strut centers [25, 28]. Outside of these regions the endothelium is assumed to be intact. In denuded regions, the flux  $J_{v,et}$  simplifies to continuity of pressure ( $p_l = p_{ses}$ ). A zero-flow condition,  $-\mathbf{n}_i \cdot \mathbf{u}_i = 0$ , where  $\mathbf{n}_i$  is the unit outward normal vector to the corresponding exterior boundary, is imposed to the left and right wall boundaries,  $\Gamma_{i,inlet}$  and  $\Gamma_{i,outlet}$ , respectively (sufficiently far from the therapeutic domain so that these boundary conditions have no effect on the results). At the perivascular side (outer boundary of the arterial wall,  $\Gamma_a$ ), a pressure of 30 mmHg [55] is applied in order to impose a pressure gradient of 70 mmHg [57] between the inner and the outer surface of the tissue. We refer the reader to Fig. 2 for a diagrammatic representation of the boundary conditions.

### 2.3.3 Modelling drug transport within the stent coating

We consider durable polymer-coated stents and assume that drug release is governed by diffusion:

$$\frac{\partial c_c}{\partial t} = \nabla \cdot (\mathbf{D}_c \nabla c_c), \quad (17)$$

where  $c_c(r, z, t)$  is the concentration of dissolved (free) drug in the coating and  $\mathbf{D}_c$  is the effective diffusion coefficient of the drug through the porous polymer. We assume that initially all the drug exists in dissolved form in the polymer coating at concentration  $C_0$ , calculated as  $M_0/V_c$ , where  $M_0$  is the initial mass of drug within the coating and  $V_c$  is the volume of the coating. Continuity of concentration and flux,  $J_{s,c}$ , of free drug across the outer boundary of the polymeric stent coating is prescribed:

$$J_{s,c} = (-\mathbf{D}_c \nabla c_c) \cdot \mathbf{n}_c = -(-\mathbf{D}_k \nabla c_k + \mathbf{u}_k c_k) \cdot \mathbf{n}_k, \quad c_c = c_k, \quad (18)$$

where the subscript  $k = \{l, ses, m\}$  represents the lumen, the SES and the media, respectively. Finally, a zero-flux condition,  $-\mathbf{n}_c \cdot (-\mathbf{D}_c \nabla c_c) = 0$  is imposed at the interface between the metallic strut and the polymer coating.

### 2.3.4 Modelling drug transport within the lumen and the arterial wall

Drug transport in the lumen is described by the unsteady advection-diffusion equation:

$$\frac{\partial c_l}{\partial t} + \mathbf{u}_l \cdot \nabla c_l = \nabla \cdot (\mathbf{D}_l \nabla c_l), \quad (19)$$

where  $c_l(r, z, t)$  is the concentration of drug in the lumen,  $\mathbf{D}_l$  is the diffusion coefficient and  $\mathbf{u}_l$  is the velocity of the blood flow in the lumen computed by the steady Navier-Stokes equations. The advection-diffusion equation is also used to model the drug transport in the intima and the adventitia:

$$\frac{\partial c_{ses}}{\partial t} + \frac{\gamma_{ses}}{\phi_{ses}} \mathbf{u}_{ses} \cdot \nabla c_{ses} = \nabla \cdot (\mathbf{D}_{ses} \nabla c_{ses}), \quad (20)$$

$$\frac{\partial c_a}{\partial t} + \frac{\gamma_a}{\phi_a} \mathbf{u}_a \cdot \nabla c_a = \nabla \cdot (\mathbf{D}_a \nabla c_a), \quad (21)$$

and the advection-diffusion-reaction equation is used to model the drug transport in the media:

$$\frac{\partial c_m}{\partial t} + \frac{\gamma_m}{\phi_m} \mathbf{u}_m \cdot \nabla c_m = \nabla \cdot (\mathbf{D}_m \nabla c_m) - \frac{\partial b_m}{\partial t}, \quad (22)$$

$$\frac{\partial b_m}{\partial t} = k_{on} c_m (b_{max} - b_m) - k_{off} b_m, \quad (23)$$

where  $c_i(r, z, t)$  denotes the volume-averaged concentration of free drug in layer  $i$ ,  $\gamma_i \leq 1$  is the hindrance coefficient,  $\phi_i$  is the porosity,  $\mathbf{u}_i$  is the transmural velocity in the porous layers computed by Darcy's law and  $\mathbf{D}_i$  is the diffusion tensor in each layer of the arterial wall. For the media layer, we consider a non-linear saturable reversible binding model (Eq. 23) to describe drug interactions with the tissue [15,25,58,59]. This model allows one to define two different states of the drug in the media layer: drug dissolved in the plasma (free drug,  $c_m(r, z, t)$ ) and drug bound to binding sites,  $b_m(r, z, t)$ . The parameters  $k_{on}$  and  $k_{off}$  are the association (binding) and dissociation (unbinding) rate constants, respectively, and  $b_{max}$  is the maximum density of binding sites. The rate constants are related through the equilibrium dissociation constant,  $K_d$ , which is defined as  $K_d = k_{off}/k_{on}$ .

The discontinuity of solute flux,  $J_s$ , across the endothelium and internal and external elastic laminae is governed by the Kedem-Katchalsky equations:

$$J_{s,j} = P_j \Delta c_j + s_j \bar{c}_j J_{v,j} \quad (24)$$

where  $P_j$  is the permeability of each semipermeable membrane,  $\Delta c_j$  is the solute concentration differential,  $s_j$  is the sieving coefficient and  $\bar{c}_j$  is computed as the weighted average of the concentrations on either side of the membrane [60]:

$$\bar{c}_{et} = \frac{1}{2}(c_l + c_{ses}) + \frac{s_{et}J_{v,et}}{12P_{et}}(c_l - c_{ses}), \quad (25)$$

$$\bar{c}_{iel} = \frac{1}{2}(c_{ses} + c_m) + \frac{s_{iel}J_{v,iel}}{12P_{iel}}(c_{ses} - c_m) \quad (26)$$

$$\bar{c}_{eel} = \frac{1}{2}(c_m + c_{adv}) + \frac{s_{eel}J_{v,eel}}{12P_{eel}}(c_m - c_{adv}). \quad (27)$$

Zero drug concentration,  $c_l = 0$ , and outflow,  $-\mathbf{n}_l \cdot (-\mathbf{D}_l \nabla c_l) = 0$ , conditions are imposed at the inlet and outlet boundaries in the lumen, respectively. Following Vairo et al. [24], the upstream and downstream boundaries of the tissue are subjected to a zero-flux condition:  $-\mathbf{n}_i \cdot (-\mathbf{D}_i \nabla c_i + \mathbf{u}_i c_i) = 0$ . Finally, a perfect sink condition,  $c_a = 0$ , was applied at the perivascular wall for the free drug. All governing equations and boundary conditions involved in the computational model have been summarised in Fig. 2.

[Fig. 2 about here.]

### 2.3.5 Drug transport model parameters

The majority of DES to date have contained either the drug paclitaxel, sirolimus or a sirolimus analogue. Sirolimus and analogues are anti-proliferative compounds that target the FK-binding protein 12 (FKBP12). This complex subsequently binds to the mammalian target of rapamycin (mTOR) and thereby interrupts the cell cycle in the G1-S phase. Paclitaxel is also an anti-proliferative compound; however, it inhibits neointimal growth by binding with and stabilising microtubules, resulting in cell-cycle arrest in the G0-G1 and G2-M phases [61]. In this work we consider both sirolimus and paclitaxel. Wherever possible, the model input parameters for sirolimus and paclitaxel are derived from experimental data available in the literature and are summarised in Table 2.

[Table 2 about here.]

## 2.4 Computational model

To analyse the effect of the mechanical expansion of DES on drug transport, an idealised numerical model is developed that accounts for the changes in the tortuosity of the arterial wall as a result of strut compression.

### 2.4.1 Model geometry

We consider initially a 2D-axisymmetric geometry of an idealised straight segment of a coronary artery where a DES is implanted (Fig. 3a). This geometry is similar to that introduced by Mongrain

et al. [22] and subsequently used by Vairo et al. [24] and Bozsak et al. [25]. The arterial wall is modelled as a three-layered structure with the subendothelial space (SES) of the intima, the media and the adventitia defined as different domains ( $\Omega_{ses}$ ,  $\Omega_m$  and  $\Omega_a$ , respectively), while the endothelium (ET), internal elastic lamina (IEL) and external elastic lamina (EEL) are treated as interfacial semipermeable membranes ( $\Gamma_{et}$ ,  $\Gamma_{iel}$  and  $\Gamma_{eel}$ , respectively). The lumen radius,  $r_l$ , and the thickness of each layer of the tissue prior to stent expansion,  $\delta_i$ , are listed in Table 3. The DES is represented by 10 polymer-coated metallic circular struts each of 0.25 mm total diameter, including a coating thickness,  $\delta_p$ , of 50  $\mu\text{m}$ , and separated by a centre-to-centre distance of 0.7 mm. A half-embedment configuration of the stent struts into the arterial is taken into account.

[Table 3 about here.]

[Fig. 3 about here.]

#### 2.4.2 Numerical methods

The commercially available software COMSOL Multiphysics 5.3a (COMSOL AB, Burlington, MA, USA) was used to create the finite element (FE) mesh and to numerically solve the coupled stent expansion/drug transport model detailed in Section 2. Three consecutive modelling steps were performed: (1) a stationary mechanical analysis was run in order to simulate the stent deployment, (2) starting from the deformed geometry computed in (1), a stationary analysis of blood flow dynamics and plasma filtration was carried out, and finally (3) a time-dependent drug transfer analysis was performed, which was coupled with the data calculated in previous steps such as the strain response of the vessel wall and the luminal and transmural flow. A sensitivity analysis was previously done in order to investigate the influence of the mesh and time step size on the results (data not shown). Different tests were made and mesh and time step independence was assumed when there was less than 1% difference in the temporal evolution of the total drug content in the media layer of the arterial wall for successive mesh and time step refinements. The computational domains were spatially discretized using a combination of triangular and quadrilateral elements, resulting in an overall mixed mesh with approximately 350,000 elements. Lagrange P3-P2 elements were used to discretize the blood dynamics problem and quadratic Lagrange elements were used to numerically approximate the mechanical, porous media and drug transport problems. A direct linear solver (MUMPS) was used to solve the stationary problems with a tolerance for the relative error of the solution of  $10^{-3}$ . The backward differentiation formula (BDF) method was the implicit method used for the time discretization of the transient drug transport problem, with variable order of accuracy varying from one (also known as the backward Euler method) to five in order to obtain better stability and variable time step size. The maximum time-step size was restricted to 1 hour. The relative and absolute tolerances were set to  $10^{-3}$  and  $10^{-4}$ , respectively. The resulting system of time-dependent partial differential equations (PDEs) were solved using a direct linear solver (PARDISO) with a nested dissection preordering algorithm. The computation time of the total simulation (the three steps described in Section 2.4.2) for each expansion case performed on 8 cores of an Intel<sup>®</sup> Core<sup>™</sup> i7-4770 CPU @ 3.40 GHz processor is about 6 hours.

### 3 Results and Discussion

In what follows, we will consider results related to five different cases: (i) uncoupled (ii) 0% expansion (iii) 10% expansion (iv) 20% expansion and (v) 30% expansion, as summarised in Table 4. In each case, the initial drug loading in the stent coating is fixed to 150  $\mu\text{g}$ . In the *uncoupled* case, we consider a straight unpressurised arterial geometry: this is essentially an extension of the model of Bozsak et al. [25] that now includes the adventitia layer. In the *0% expansion model* the artery is now pressurised, causing a reduction in thickness of the arterial tissue, but overexpansion of the vessel caused by the stent is not considered. The remaining cases simulate a pressurised artery as well as a further deformation over the stented portion due to expansion of the stent. With the exception of case (i), all of our simulations result in changes to drug transport parameters as outlined in Section 2.

[Table 4 about here.]

In order to compare results between the different cases, we will consider the temporal profiles of drug content and spatial profiles of local drug concentration in tissue. The total drug content in each layer of the tissue (presented as  $\mu\text{g}$  drug per g of tissue) at any instant is calculated as [20, 36]:

$$DC_i(t) = \frac{MW_{drug}}{V_i \rho_i} \int_{V_i} (c_i + b_i) dV_i, \quad (28)$$

where  $V_i$  is the volume of layer  $i$ , that falls within the therapeutic domain considering  $a < z < b$ , with the origin of the computational geometry placed between the two central struts and with  $a = -7.5w_s$  and  $b = 7.5w_s$ , where  $w_s$  is the interstrut distance (see Fig. 3);  $MW_{drug}$  is the molecular weight of the drug (sirolimus or paclitaxel) and;  $\rho_i$  is the density of wet arterial layer tissue. In the absence of experimental data on a layer-specific basis, we assume a constant density across the three arterial wall layers (see Table 2). Moreover, since binding site saturation has been linked with efficacy [20, 36] we further calculate the % of binding sites that are saturated as a function of time:

$$Binding\ sites\ \% \ saturation(t) = \frac{100}{V_i b_{max}} \int_{V_i} (b_i) dV_i. \quad (29)$$

Note that in this model, binding is only considered in the media layer, therefore the % saturation in the SES and in the adventitia will be zero.

In Fig. 4 we plot temporal profiles of drug content (DC) of two drugs, sirolimus or paclitaxel, within each layer of the arterial wall for cases (i)-(v). The plots show that, in the media and the adventitia, the peak DC decreases with stent expansion, however in the SES, the peak DC increases with the level of expansion. The time that the peak DC occurs increases sequentially moving from the SES to the adventitia and there is a short delay before drug enters the adventitia, consistent with the time taken for drug to traverse the media. Similar trends are observed between sirolimus and paclitaxel, although the values of DC differ as a result of drug-specific binding and transport parameters. Interestingly, the DC of sirolimus is higher than paclitaxel in the SES and media, but lower in the adventitia.

In Fig. 5 we separate-out free DC from bound DC in the media for each drug. We observe that, for each drug, the peak free DC decreases with level of expansion while there is a negligible effect on peak bound DC. The implication is that expansion has a more pronounced effect on media free drug concentrations. High levels of binding site saturation are achieved for both sirolimus ( $\approx 70\%$ ) and paclitaxel ( $\approx 75-80\%$ ) rapidly, before a steady decline in saturation levels with time. The decline is more rapid for paclitaxel. Figs. 4-5 demonstrate that the effect of stent expansion on drug transport in the arterial wall is dependent not only on the specific layer in question, but also on the particular drug. Generally speaking, the effect of expansion is more prominent in the case of paclitaxel, particularly so in the adventitia layer of the arterial wall.

[Fig. 4 about here.]

[Fig. 5 about here.]

While DC provides a useful gross measure to effect comparisons, it is also important to consider the impact of local drug concentrations, which are linked to the biological effect of the drug, in order to assess whether drug concentrations locally are at therapeutic (and not toxic) levels. The study of local drug concentrations is also relevant for the design of effective drug delivery modalities [62]. In Fig. 6 we display spatially-varying profiles of total (free plus bound) local sirolimus concentration in the arterial wall, calculated as  $(c_i + b_i) \frac{MW_{drug}}{\rho_i}$ , at four different times across a radial section between the middle struts (i.e. between the 5th and 6th struts). The greatest differences between the four cases are observed at early times, where the peak sirolimus local concentration decreases with level of expansion. When the drug reaches the media/adventitia boundary, there is a sharp jump in the spatial profiles resulting from the contrast in material properties between the layers, described through the Kedem-Katchalsky equations. As time progresses, the higher drug retention in the media layer is evident compared with the adventitia. Our model also enables us to generate 2D plots of local drug concentration.

In Fig. 7 we show the spatial distribution of the total local concentration of sirolimus in the therapeutic domain at various time points across 7 days for the 0% and 30% expansion cases. The five time points after stent implantation shown are:  $t = 10$  min,  $t = 1$  hour,  $t = 4$  hours,  $t = 24$  hours and  $t = 7$  days. We observe that at early times the concentration is higher close to the stent struts and relatively lower close to the lumen between struts. After 1 hour of the stent implantation, the plots show the drug progression through the media layer with time and after 4 hours the concentration distribution pattern in the arterial wall is more homogeneous. After 1 day, the concentration level of drug in the tissue has already dropped approximately by an order of magnitude in the media and is almost 40 times lower in the adventitia compared to the maximum concentration reached in this layer. After a week, the concentration level in the media is approximately 20 times lower than the maximum concentration value. In general, similar trends are observed for both cases of expansion, but with lower levels of concentration when expansion increases. A comparison between the spatial distribution in the tissue of sirolimus and paclitaxel for each expansion case and the corresponding tables with the maximum values at each time point may be found in the supplementary material.

[Fig. 6 about here.]

[Fig. 7 about here.]

In Figs. 8, 9 and 10 we separate-out the free and bound local sirolimus concentration. From these plots we deduce that, in the early stages, the total local drug concentration profiles are characterized by rapid infiltration of drug into the SES followed by rapid diffusion into the media (these early profiles are governed by the free local drug concentration). However, as time progresses, the total local drug concentration profiles are dominated by the bound local drug concentration. There is little difference between binding site saturation levels as we increase level of expansion. However, at early times, expansion has the effect of leading to binding site saturation deeper into the wall. In order to probe this further, in Figs. 11 and 12 we present plots showing how the radial and longitudinal diffusion coefficients ( $D_r$  and  $D_z$ , respectively), magnitude of the radial component of flow ( $u_r$ ) and radial Peclet number ( $Pe_r = u_r \delta_m / D_r$ ) vary across the media layer for the various levels of expansion considered. Fig. 11a confirms that as we increase the level of expansion, we decrease the radial diffusion coefficient, with differences greater closer to the intima. The dependence of the longitudinal diffusion coefficient on expansion is more complex, increasing with expansion close to the intima before decreasing with expansion close to the adventitia as can be seen in Fig. 11b. The level of expansion also has an influence on the resulting flow-field in the tissue (Fig. 12a): higher radial flow speed is observed with increasing levels of expansion. When we consider the radial Peclet number (Fig. 12b) we observe a similar profile to that of radial flow speed (Fig. 12a), confirming that transport across the wall, in all cases, is dominated by advection. Therefore, despite the relatively modest reduction in radial diffusion coefficient with expansion, it is primarily advection driven by the pressure gradient across the wall that governs radial drug transport. These findings support the relatively modest variation in temporal and spatial profiles of content of drug in Figs. 4-10. Importantly, we note that given the low value of the radial Peclet number (of order 1), a relatively small change to the flow field could tip the balance back in favour of diffusion, and in this case the observed changes in drug diffusion as a result of mechanical expansion will be of more significance. Similar trends are observed for paclitaxel, but with greater differences between cases (i)-(v). The corresponding plots for paclitaxel may be found in the supplementary material.

[Fig. 8 about here.]

[Fig. 9 about here.]

[Fig. 10 about here.]

[Fig. 11 about here.]

[Fig. 12 about here.]

## 4 Limitations

We would like to emphasize that there are a number of limitations in this work, as we now discuss. Regarding the geometry of the model, a 2D axysymmetric geometry corresponding to an idealised representation of a straight segment of a healthy coronary artery has been considered in this study. This could be improved using more realistic geometries of arteries (curved segments, bifurcations

or directly 3D patient-specific geometries obtained from medical images) and devices (i.e. complex geometries of commercial DES). However, such models considerably increase the computational cost of the simulations and detract from the key objective which was to study the effect of coupling mechanics-drug transport. Moreover, there is growing evidence that disease composition may well have an impact on drug release and subsequent tissue distribution [63], however in line with most of the computational models of drug transport in arteries published in the literature, we neglect the existence of atheroma plaque in this work.

The large number of parameters involved in the model were obtained from existing experimental data or other computational models. These data are taken from different species and may not be representative of the corresponding parameters in human tissue. Moreover, there is a lack of transport and reaction parameters for the adventitia layer, therefore these parameters had to be estimated.

Our proposed description of the blood flow (steady Newtonian with inlet Poiseuille velocity profile and outlet fixed pressure boundary conditions) aligns with the current state of the art model which couples luminal flow with drug release from stents and tissue binding [25], as well as many other groups in the field [22–25]. Whilst we accept that in reality we will have pulsatile flow, we point out that the focus of this study is on drug distribution in arterial tissue, rather than on accurately reproducing flow patterns in the lumen. We cite evidence from the literature which shows that 'pulsatility contributes minimally to drug deposition for a well-apposed strut' [64]. Moreover, the pulsatile flow is characterized by much smaller temporal scales than the temporal scale of the advection-diffusion-reaction processes which govern drug transport within the arterial wall, therefore, the time dependence mainly due to the cardiac pulsatile flow was finally neglected in this work.

In terms of modelling drug transport within the stent coating, in line with the vast majority of models in the literature, simple diffusion model is considered in this work. However, depending on the particular stent, drug and coating under consideration, more complex nonlinear model that accounts for the combined effects of diffusion, dissolution and solubility in the polymer coating [19] may be required in order to describe drug release from the stent. In the literature we can find a wide range for diffusion coefficients of the drug in the polymeric coating of the stent, representing the range from fast- to slow-release kinetics. These values range from  $10^{-13}$  to  $10^{-17}$   $\text{m}^2 \cdot \text{s}^{-1}$  [25]. Moreover, there are a large number of stents on the market ranging from durable polymer coated stents, to polymer free and biodegradable stents and the release kinetics can vary considerably between these different types. In this work, we assume a typical fast-release stent taking a diffusion coefficient of  $10^{-13}$   $\text{m}^2 \cdot \text{s}^{-1}$  in all simulations.

In terms of modelling drug transport within the arterial wall, a single phase nonlinear saturable reversible binding model is taken into account. Therefore, in this model we do not take into account the effect of binding as two separate phases (drug bound to specific receptors and non-specific general extracellular matrix sites), the benefits and drawbacks of which are discussed in [6]. In order to simulate stent deployment, vessel pressurization and displacement have been performed in a single computation step. A more realistic and challenging approach would be to perform this in two separate stages.

Finally, we appreciate the importance of validating computational models such as ours against ex-

perimental data. However, to the best of our knowledge, there is a lack of experimental tests in the available literature that relate the level of deformation due to stenting, and the consequent modification of material properties of the tissue, with the drug content within the arterial wall. We would hope that this work would inspire the generation of suitable experimental data to validate the work.

## 5 Conclusions

In this paper, we have provided a comprehensive study of the effect of stent mechanical expansion on the drug transport properties of a three-layer arterial wall described as an anisotropic, hyperelastic material. We have established relationships between mechanical force generated through device expansion and alteration in drug diffusion coefficients within the arterial wall and performed simulations to quantify the impact of such alterations in spatio-temporal drug release and tissue uptake. Our findings demonstrate that mechanical expansion can have an influence on the effective diffusion coefficients of drugs in arterial tissue, with the overall influence on drug transport through the arterial wall dependent on the radial Peclet number that is derived from these diffusion coefficients. Since current computational models typically make use of drug diffusion coefficients that have been derived from static tissue experiments (i.e. not subjected to mechanical expansion), these models are likely to be under- or over-estimating drug transport and retention in arterial tissue. Finally, we remark that our findings may also be of importance to other forms of localised arterial drug delivery, such as through drug coated balloons (DCBs). The key difference with DCBs would appear to be a time-varying dependence on drug transport parameters, coinciding with inflation and deflation of the balloon.

**Acknowledgments:** Financial support for this research was provided by the Spanish Ministry of Economy and Competitiveness through research project DPI2016-76630-C2-1-R and grant number BES-2014-069737; the Department of Industry and Innovation (Government of Aragon) through the research group Grant T24-17R (Fondo Social Europeo) and research project LMP121-18 and; the Instituto de Salud Carlos III (ISCIII) through the CIBER initiative.

## References

- [1] Naghavi M, Abajobir AA, Abbafati C, Abbas KM, Abd-Allah F, Abera SF, et al. Global, regional, and national age-sex specific mortality for 264 causes of death, 1980–2016: a systematic analysis for the Global Burden of Disease Study 2016. *The Lancet*. 2017;390(10100):1151–1210.
- [2] Alfonso F, Byrne RA, Rivero F, Kastrati A. Current treatment of in-stent restenosis. *Journal of the American College of Cardiology*. 2014;63(24):2659–2673.
- [3] Buccheri D, Piraino D, Andolina G, Cortese B. Understanding and managing in-stent restenosis: a review of clinical data, from pathogenesis to treatment. *Journal of Thoracic Disease*. 2016;8(10):E1150.
- [4] Byrne RA, Joner M, Kastrati A. Stent thrombosis and restenosis: what have we learned and where are we going? The Andreas Grüntzig Lecture ESC 2014. *European Heart Journal*. 2015;36(47):3320–3331.

- [5] Conway C, Sharif F, McGarry J, McHugh P. A computational test-bed to assess coronary stent implantation mechanics using a population-specific approach. *Cardiovascular Engineering and Technology*. 2012;3(4):374–387.
- [6] McGinty S, Pontrelli G. On the role of specific drug binding in modelling arterial eluting stents. *Journal of Mathematical Chemistry*. 2016;54(4):967–976.
- [7] Migliavacca F, Petrini L, Montanari V, Quagliana I, Auricchio F, Dubini G. A predictive study of the mechanical behaviour of coronary stents by computer modelling. *Medical Engineering & Physics*. 2005;27(1):13–18.
- [8] Lally C, Dolan F, Prendergast P. Cardiovascular stent design and vessel stresses: a finite element analysis. *Journal of Biomechanics*. 2005;38(8):1574–1581.
- [9] Kioussis DE, Gasser TC, Holzapfel GA. A numerical model to study the interaction of vascular stents with human atherosclerotic lesions. *Annals of Biomedical Engineering*. 2007;35(11):1857–1869.
- [10] Zahedmanesh H, Kelly DJ, Lally C. Simulation of a balloon expandable stent in a realistic coronary artery: Determination of the optimum modelling strategy. *Journal of Biomechanics*. 2010;43(11):2126–2132.
- [11] García A, Peña E, Martínez M. Influence of geometrical parameters on radial force during self-expanding stent deployment. Application for a variable radial stiffness stent. *Journal of the Mechanical Behavior of Biomedical Materials*. 2012;10:166–175.
- [12] Conway C, McGarry J, McHugh P. Modelling of atherosclerotic plaque for use in a computational test-bed for stent angioplasty. *Annals of Biomedical Engineering*. 2014;42(12):2425–2439.
- [13] McGinty S. A decade of modelling drug release from arterial stents. *Mathematical biosciences*. 2014;257:80–90.
- [14] Pontrelli G, de Monte F. Mass diffusion through two-layer porous media: an application to the drug-eluting stent. *International Journal of Heat and Mass Transfer*. 2007;50(17-18):3658–3669.
- [15] Tzafriri AR, Levin AD, Edelman ER. Diffusion-limited binding explains binary dose response for local arterial and tumour drug delivery. *Cell proliferation*. 2009;42(3):348–363.
- [16] Pontrelli G, de Monte F. A multi-layer porous wall model for coronary drug-eluting stents. *International Journal of Heat and Mass Transfer*. 2010;53(19-20):3629–3637.
- [17] McGinty S, McKee S, Wadsworth RM, McCormick C. Modelling drug-eluting stents. *Mathematical medicine and biology: a journal of the IMA*. 2010;28(1):1–29.
- [18] d’Errico M, Sammarco P, Vairo G. Analytical modeling of drug dynamics induced by eluting stents in the coronary multi-layered curved domain. *Mathematical Biosciences*. 2015;267:79–96.
- [19] McGinty S, Pontrelli G. A general model of coupled drug release and tissue absorption for drug delivery devices. *Journal of controlled release*. 2015;217:327–336.
- [20] McKittrick C, McKee S, Kennedy S, Oldroyd K, Wheel M, Pontrelli G, et al. Combining mathematical modelling with in vitro experiments to predict in vivo drug-eluting stent performance. *Journal of Controlled Release*. 2019;.
- [21] Zunino P. Multidimensional pharmacokinetic models applied to the design of drug-eluting stents. *Cardiovascular Engineering: An International Journal*. 2004;4(2):181–191.

- [22] Mongrain R, Leask R, Brunette J, Faik I, Bulman-Feleming N, Nguyen T. Numerical modeling of coronary drug eluting stents. *Studies in Health Technology and Informatics*. 2005;113:443–458.
- [23] Mongrain R, Faik I, Leask RL, Rodés-Cabau J, Larose É, Bertrand OF. Effects of diffusion coefficients and struts apposition using numerical simulations for drug eluting coronary stents. *Journal of Biomechanical Engineering*. 2007;129(5):733–742.
- [24] Vairo G, Cioffi M, Cottone R, Dubini G, Migliavacca F. Drug release from coronary eluting stents: a multidomain approach. *Journal of biomechanics*. 2010;43(8):1580–1589.
- [25] Bozsak F, Chomaz JM, Barakat AI. Modeling the transport of drugs eluted from stents: physical phenomena driving drug distribution in the arterial wall. *Biomechanics and Modeling in Mechanobiology*. 2014;13(2):327–347.
- [26] Denny WJ, Walsh MT. Numerical modelling of mass transport in an arterial wall with anisotropic transport properties. *Journal of Biomechanics*. 2014;47(1):168–177.
- [27] Denny WJ, Walsh MT. Numerical modelling of the physical factors that affect mass transport in the vasculature at early time periods. *Medical Engineering & Physics*. 2014;36(3):308–317.
- [28] Bozsak F, Gonzalez-Rodriguez D, Sternberger Z, Belitz P, Bewley T, Chomaz JM, et al. Optimization of drug delivery by drug-eluting stents. *PLoS One*. 2015;10(6):e0130182.
- [29] Ferreira JA, Gonçalves L, Naghipoor J, de Oliveira P, Rabczuk T. The influence of atherosclerotic plaques on the pharmacokinetics of a drug eluted from bioabsorbable stents. *Mathematical biosciences*. 2017;283:71–83.
- [30] Tzafiriri AR, Garcia-Polite F, Li X, Keating J, Balaguer JM, Zani B, et al. Defining drug and target protein distributions after stent-based drug release: Durable versus deployable coatings. *Journal of Controlled Release*. 2018;274:102–108.
- [31] Ferreira JA, Gonçalves L, Naghipoor J, de Oliveira P, Rabczuk T. The effect of plaque eccentricity on blood hemodynamics and drug release in a stented artery. *Medical Engineering & Physics*. 2018;60:47–60.
- [32] Migliavacca F, Gervaso F, Prosi M, Zunino P, Minisini S, Formaggia L, et al. Expansion and drug elution model of a coronary stent. *Computer Methods in Biomechanics and Biomedical Engineering*. 2007;10(1):63–73.
- [33] Zunino P, D'Angelo C, Petrini L, Vergara C, Capelli C, Migliavacca F. Numerical simulation of drug eluting coronary stents: mechanics, fluid dynamics and drug release. *Computer Methods in Applied Mechanics and Engineering*. 2009;198(45-46):3633–3644.
- [34] Feenstra PH, Taylor CA. Drug transport in artery walls: a sequential porohyperelastic-transport approach. *Computer Methods in Biomechanics and Biomedical Engineering*. 2009;12(3):263–276.
- [35] Cutrì E, Zunino P, Morlacchi S, Chiastra C, Migliavacca F. Drug delivery patterns for different stenting techniques in coronary bifurcations: a comparative computational study. *Biomechanics and Modeling in Mechanobiology*. 2013;12(4):657–669.
- [36] Tzafiriri AR, Groothuis A, Price GS, Edelman ER. Stent elution rate determines drug deposition and receptor-mediated effects. *Journal of controlled release*. 2012;161(3):918–926.

- [37] Zhu X, Braatz RD. A mechanistic model for drug release in PLGA biodegradable stent coatings coupled with polymer degradation and erosion. *Journal of Biomedical Materials Research Part A*. 2015;103(7):2269–2279.
- [38] Carew TE, Vaishnav RN, Patel DJ. Compressibility of the arterial wall. *Circulation Research*. 1968;23(1):61–68.
- [39] Holzapfel GA, Stadler M, Gasser TC. Changes in the mechanical environment of stenotic arteries during interaction with stents: computational assessment of parametric stent designs. *Journal of Biomechanical Engineering*. 2005;127(1):166–180.
- [40] Gasser TC, Ogden RW, Holzapfel GA. Hyperelastic modelling of arterial layers with distributed collagen fibre orientations. *Journal of the Royal Society Interface*. 2006;3(6):15–35.
- [41] Spencer A. Part III. Theory of invariants. *Continuum Physics*. 1971;1:239–353.
- [42] Gundiah N, Ratcliffe MB, Pruitt LA. The biomechanics of arterial elastin. *Journal of the Mechanical Behavior of Biomedical Materials*. 2009;2(3):288–296.
- [43] Lillie M, Shadwick R, Gosline J. Mechanical anisotropy of inflated elastic tissue from the pig aorta. *Journal of Biomechanics*. 2010;43(11):2070–2078.
- [44] Holzapfel GA, Gasser TC, Ogden RW. A new constitutive framework for arterial wall mechanics and a comparative study of material models. *Journal of Elasticity and the Physical Science of Solids*. 2000;61(1-3):1–48.
- [45] McGarry J, O'Donnell B, McHugh P, McGarry J. Analysis of the mechanical performance of a cardiovascular stent design based on micromechanical modelling. *Computational Materials Science*. 2004;31(3-4):421–438.
- [46] Hopkins C, McHugh P, McGarry J. Computational investigation of the delamination of polymer coatings during stent deployment. *Annals of Biomedical Engineering*. 2010;38(7):2263–2273.
- [47] Schiavone A, Zhao L, Abdel-Wahab AA. Effects of material, coating, design and plaque composition on stent deployment inside a stenotic artery-finite element simulation. *Materials Science and Engineering: C*. 2014;42:479–488.
- [48] O'Connell BM, Walsh MT. Arterial mass transport behaviour of drugs from drug eluting stents. In: *Biomedical Science, Engineering and Technology*. IntechOpen; 2012. .
- [49] Cussler EL. *Diffusion: mass transfer in fluid systems*. Cambridge university press; 2009.
- [50] O'Connell BM, McGloughlin TM, Walsh MT. Factors that affect mass transport from drug eluting stents into the artery wall. *Biomedical Engineering Online*. 2010;9(1):15.
- [51] Hwang CW, Edelman ER. Arterial ultrastructure influences transport of locally delivered drugs. *Circulation Research*. 2002;90(7):826–832.
- [52] Levin AD, Vukmirovic N, Hwang CW, Edelman ER. Specific binding to intracellular proteins determines arterial transport properties for rapamycin and paclitaxel. *Proceedings of the National Academy of Sciences of the United States of America*. 2004;101(25):9463–9467.
- [53] O'Connell BM, Walsh MT. Demonstrating the influence of compression on artery wall mass transport. *Annals of Biomedical Engineering*. 2010;38(4):1354–1366.

- [54] Formaggia L, Quarteroni A, Veneziani A. *Cardiovascular Mathematics: Modeling and simulation of the circulatory system*. vol. 1. Formaggia L, Quarteroni A, Veneziani A, editors. Springer Science & Business Media; 2010.
- [55] Ai L, Vafai K. A coupling model for macromolecule transport in a stenosed arterial wall. *International Journal of Heat and Mass Transfer*. 2006;49(9-10):1568–1591.
- [56] Kedem O, Katchalsky A. Thermodynamic analysis of the permeability of biological membranes to non-electrolytes. *Biochimica et Biophysica Acta*. 1958;27:229–246.
- [57] Meyer G, Merval R, Tedgui A. Effects of pressure-induced stretch and convection on low-density lipoprotein and albumin uptake in the rabbit aortic wall. *Circulation Research*. 1996;79(3):532–540.
- [58] Kolachalama VB, Pacetti SD, Franses JW, Stankus JJ, Zhao HQ, Shazly T, et al. Mechanisms of tissue uptake and retention in zotarolimus-coated balloon therapy. *Circulation*. 2013;127(20):2047–2055.
- [59] McGinty S, McKee S, McCormick C, Wheel M. Release mechanism and parameter estimation in drug-eluting stent systems: analytical solutions of drug release and tissue transport. *Mathematical Medicine and Biology: a Journal of the IMA*. 2015;32(2):163–186.
- [60] Levitt DG. General continuum analysis of transport through pores. I. Proof of Onsager's reciprocity postulate for uniform pore. *Biophysical Journal*. 1975;15(6):533–551.
- [61] Martin DM, Boyle FJ. Drug-eluting stents for coronary artery disease: a review. *Medical Engineering & Physics*. 2011;33(2):148–163.
- [62] Hwang CW, Wu D, Edelman ER. Physiological transport forces govern drug distribution for stent-based delivery. *Circulation*. 2001;104(5):600–605.
- [63] McKittrick C, Kennedy S, Oldroyd K, McGinty S, McCormick C. Modelling the impact of atherosclerosis on drug release and distribution from coronary stents. *Annals of biomedical engineering*. 2016;44(2):477–487.
- [64] O'Brien CC, Kolachalama VB, Barber TJ, Simmons A, Edelman ER. Impact of flow pulsatility on arterial drug distribution in stent-based therapy. *Journal of controlled release*. 2013;168(2):115–124.
- [65] Holzapfel GA, Sommer G, Gasser CT, Regitnig P. Determination of layer-specific mechanical properties of human coronary arteries with nonatherosclerotic intimal thickening and related constitutive modeling. *American Journal of Physiology-Heart and Circulatory Physiology*. 2005;289(5):H2048–H2058.
- [66] Karner G, Perktold K, Zehentner HP. Computational modeling of macromolecule transport in the arterial wall. *Computer Methods in Biomechanics and Biomedical Engineering*. 2001;4(6):491–504.
- [67] Curry FRE. Mechanics and thermodynamics of transcapillary exchange. *Handbook of Physiology*. 1984;p. 309–374.
- [68] Dodge Jr JT, Brown BG, Bolson EL, Dodge HT. Lumen diameter of normal human coronary arteries. Influence of age, sex, anatomic variation, and left ventricular hypertrophy or dilation. *Circulation*. 1992;86(1):232–246.
- [69] Creel CJ, Lovich MA, Edelman ER. Arterial paclitaxel distribution and deposition. *Circulation Research*. 2000;86(8):879–884.

<b>a. ARTERIAL WALL</b>								
Material	Model	$\mu$ (kPa)	$k_1$ (kPa)	$k_2$ (-)	$\kappa$ (-)	$\beta$ ( $^\circ$ )	NRMSE	Reference
Intima	Gasser et al. [40]	26.16	10485.17	20.00	0.165	50.02	0.0249	fitted to [65]
Media	Gasser et al. [40]	1.93	149.10	51.74	0.262	37.47	0.0157	fitted to [65]
Adventitia	Gasser et al. [40]	8.17	695.61	604.79	0.265	60.33	0.0298	fitted to [65]

<b>b. STENT STRUTS</b>								
Material	Model	$E$ (MPa)	$\nu$ (-)	$\sigma_y$ (MPa)	$\sigma_u$ (MPa)	$\epsilon_u$ (-)	Reference	
Stainless steel 316L	Elasto-plastic	$2 \cdot 10^5$	0.28	264	584	0.247	[5,45]	

<b>c. STENT COATING</b>							
Material	Model	$E$ (MPa)	$\nu$	$\sigma_y$ (MPa)	$E_t$ (MPa)	Reference	
PC-based polymer	Bilinear elastic	240	0.5	16	7.7	[46,47]	

Table 1

(a) Material parameters of the Gasser et al. [40] strain energy function (SEF) for the different layers of the arterial wall. The normalised root mean square error (NRMSE) is a measure of the accuracy of the fit. (b) Coefficients of the elasto-plastic material model used to describe the behaviour of the stent struts. (c) Values of the bilinear elasto-plastic model parameters for the phosphorylcholine polymer coating.

Parameter	Description	Value	Reference
$\Delta p$	Pressure difference between lumen and adventitia	70 mmHg	[57]
$Re_l$	Luminal Reynolds number	400	[54]
$\rho_b$	Blood density	1060 kg·m <sup>-3</sup>	[25]
$\rho_p$	Plasma density	1060 kg·m <sup>-3</sup>	[25]
$\mu_b$	Blood dynamic viscosity	3.5 · 10 <sup>-3</sup> Pa·s	[66]
$\mu_p$	Plasma dynamic viscosity	7.2 · 10 <sup>-4</sup> Pa·s	[21]
$\rho_i$	Density of wet arterial tissue	983 kg·m <sup>-3</sup>	[36]
$\phi_{ses}$	Porosity of the intima	0.983	[55]
$\phi_m$	Porosity of the media	0.258	[55]
$\phi_a$	Porosity of the adventitia	0.85	[18]
$\gamma_{ses}$	Hindrance coefficient in the intima	1	Calculated from [25]
$\gamma_m$	Hindrance coefficient in the media	0.845	Calculated from [25, 54, 67]
$\gamma_a$	Hindrance coefficient in the adventitia	1	Estimated
$\kappa_{ses}$	Darcy permeability in the intima	2.2 · 10 <sup>-16</sup> m <sup>2</sup>	[55]
$\kappa_m$	Darcy permeability in the media	2 · 10 <sup>-18</sup> m <sup>2</sup>	[21]
$\kappa_a$	Darcy permeability in the adventitia	2 · 10 <sup>-18</sup> m <sup>2</sup>	[24]
$L_{p,et}$	Hydraulic conductivity of endothelium	2.2 · 10 <sup>-12</sup> m <sup>2</sup> ·s·kg <sup>-1</sup>	[25]
$L_{p,iel}$	Hydraulic conductivity of IEL	2.2 · 10 <sup>-9</sup> m <sup>2</sup> ·s·kg <sup>-1</sup>	[25]
$L_{p,eel}$	Hydraulic conductivity of EEL	2.2 · 10 <sup>-9</sup> m <sup>2</sup> ·s·kg <sup>-1</sup>	Estimated
$M_0$	Drug dose in the coating	150 $\mu$ g	Estimated
$D_c$	Effective diffusion coefficient in the coating	10 <sup>-13</sup> m <sup>2</sup> ·s <sup>-1</sup>	[22]
<b>SIROLIMUS</b>			
$D_l$	Effective diffusion coefficient in the lumen	4.1 · 10 <sup>-12</sup> m <sup>2</sup> ·s <sup>-1</sup>	[25]
$D_{ses}$	Effective diffusion coefficient in the intima	1.67 · 10 <sup>-11</sup> m <sup>2</sup> ·s <sup>-1</sup>	[25]
$D_{m,r}$	Effective radial diffusion coefficient in the media	7 · 10 <sup>-12</sup> m <sup>2</sup> ·s <sup>-1</sup>	[52]
$D_{m,z}$	Effective axial diffusion coefficient in the media	4 · 10 <sup>-11</sup> m <sup>2</sup> ·s <sup>-1</sup>	[52]
$D_a$	Effective diffusion coefficient in the adventitia	4 · 10 <sup>-12</sup> m <sup>2</sup> ·s <sup>-1</sup>	Estimated
$P_{et}$	Permeability of endothelium	3.6 · 10 <sup>-6</sup> m·s <sup>-1</sup>	[25]
$P_{iel}$	Permeability of IEL	9.6 · 10 <sup>-6</sup> m·s <sup>-1</sup>	[25]
$P_{eel}$	Permeability of EEL	9.6 · 10 <sup>-6</sup> m·s <sup>-1</sup>	Estimated
$s_{et}$	Sieving coefficient in the endothelium	0.855	[25]
$s_{iel}$	Sieving coefficient in the IEL	1	[25]
$s_{eel}$	Sieving coefficient in the EEL	1	Estimated
$K_d$	Equilibrium dissociation constant	2.6 · 10 <sup>-3</sup> mol·m <sup>-3</sup>	[15]
$k_{on}$	Drug binding rate constant	2 m <sup>3</sup> ·mol <sup>-1</sup> ·s <sup>-1</sup>	[15]
$k_{off}$	Drug unbinding rate constant	5.2 · 10 <sup>-3</sup> s <sup>-1</sup>	[6]
$b_{max}$	Total binding site density	0.366 mol·m <sup>-3</sup>	[15]
$MW_{sir}$	Molecular weight	914.172 g·mol <sup>-1</sup>	[52]
<b>PACLITAXEL</b>			
$D_l$	Effective diffusion coefficient in the lumen	4.2 · 10 <sup>-12</sup> m <sup>2</sup> ·s <sup>-1</sup>	[25]
$D_{ses}$	Effective diffusion coefficient in the intima	1.7 · 10 <sup>-11</sup> m <sup>2</sup> ·s <sup>-1</sup>	[25]
$D_{m,r}$	Effective radial diffusion coefficient in the media	2 · 10 <sup>-12</sup> m <sup>2</sup> ·s <sup>-1</sup>	[52]
$D_{m,z}$	Effective axial diffusion coefficient in the media	5 · 10 <sup>-11</sup> m <sup>2</sup> ·s <sup>-1</sup>	[52]
$D_a$	Effective diffusion coefficient in the adventitia	4 · 10 <sup>-12</sup> m <sup>2</sup> ·s <sup>-1</sup>	[24]
$P_{et}$	Permeability of endothelium	3 · 10 <sup>-6</sup> m·s <sup>-1</sup>	[25]
$P_{iel}$	Permeability of IEL	9.8 · 10 <sup>-6</sup> m·s <sup>-1</sup>	[25]
$P_{eel}$	Permeability of EEL	9.8 · 10 <sup>-6</sup> m·s <sup>-1</sup>	Estimated
$s_{et}$	Sieving coefficient in the endothelium	0.86	[25]
$s_{iel}$	Sieving coefficient in the IEL	1	[25]
$s_{eel}$	Sieving coefficient in the EEL	1	Estimated
$K_d$	Equilibrium dissociation constant	3.1 · 10 <sup>-3</sup> mol·m <sup>-3</sup>	[15]
$k_{on}$	Drug binding rate constant	0.17 m <sup>3</sup> ·mol <sup>-1</sup> ·s <sup>-1</sup>	Calculated from [15]
$k_{off}$	Drug unbinding rate constant	5.27 · 10 <sup>-4</sup> s <sup>-1</sup>	Calculated from [15]
$b_{max}$	Total binding site density	0.127 mol·m <sup>-3</sup>	[15]
$MW_{ptx}$	Molecular weight	853.906 g·mol <sup>-1</sup>	[52]

Table 2

List of parameters related to the drug transport model.

Parameter	Description	Value	Reference
$r_l$	Lumen radius	2.0 mm	[68]
$\delta_{ses}$	Intima thickness	0.01 mm	[66]
$\delta_m$	Media thickness	0.5 mm	[32]
$\delta_a$	Adventitia thickness	0.4 mm	[69]
$d_{strut}$	Strut diameter	0.15 mm	[22]
$\delta_p$	Polymeric coating thickness	0.05 mm	[22]
$w_s$	Interstrut distance	0.7 mm	[22]

Table 3  
List of parameters related to the geometrical model prior to stent expansion

Case	Description	Pressurised artery?	Lumen radius in stented region	Lumen radius in unstented region
(i)	Uncoupled	No	2.0 mm	2.0 mm
(ii)	0 % expansion	Yes (P=100 mmHg)	2.0 mm	2.0 mm
(iii)	10 % expansion	Yes (P=100 mmHg)	2.2 mm	2.0 mm
(iv)	20 % expansion	Yes (P=100 mmHg)	2.4 mm	2.0 mm
(v)	30 % expansion	Yes (P=100 mmHg)	2.6 mm	2.0 mm

**Table 4**

Summary of the five different cases considered in the simulations. In each case, the initial drug loading is 150  $\mu\text{g}$ .

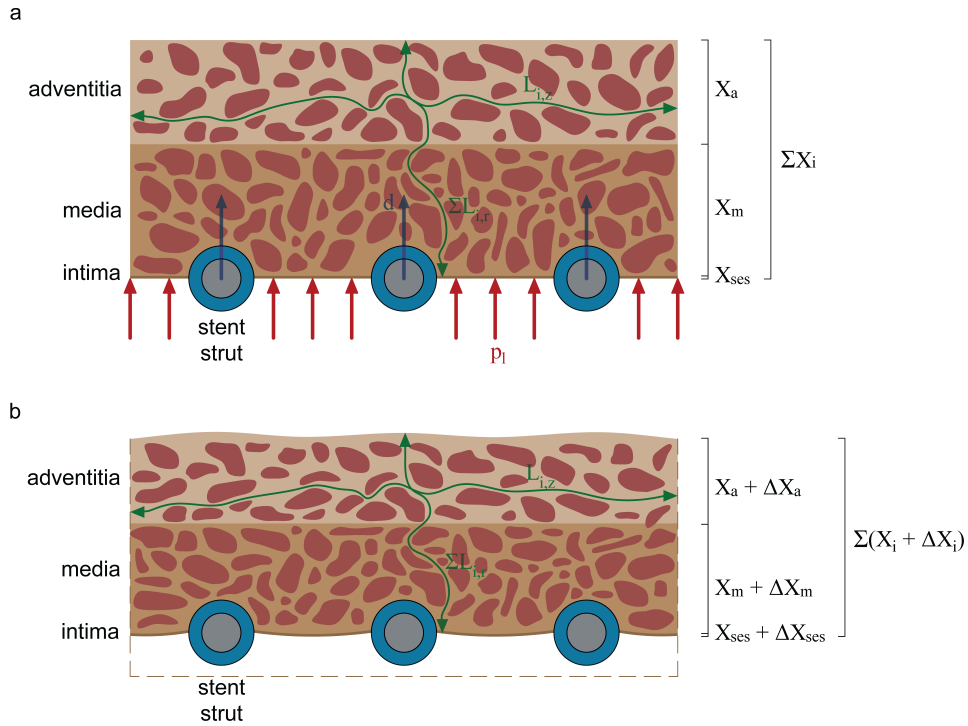


Fig. 1. Schematic showing the influence of stent expansion on tortuosity. (a) Prior to stent expansion, the tortuous path length in the radial direction through the three layers of the tissue is given by  $\sum L_{i,r}$ , while the path length in the longitudinal is given by  $L_{i,z}$ , where the subscript  $i = \{ses, m, a\}$  denotes the subendothelial space of the intima, the media and the adventitia, respectively. The total thickness of the wall is given by  $\sum X_i$ . (b) After stent expansion, the total deformed thickness of the wall is  $\sum (X_i + \Delta X_i)$ , where  $\Delta X_i > 0$  denotes elongation and  $\Delta X_i < 0$  contraction.

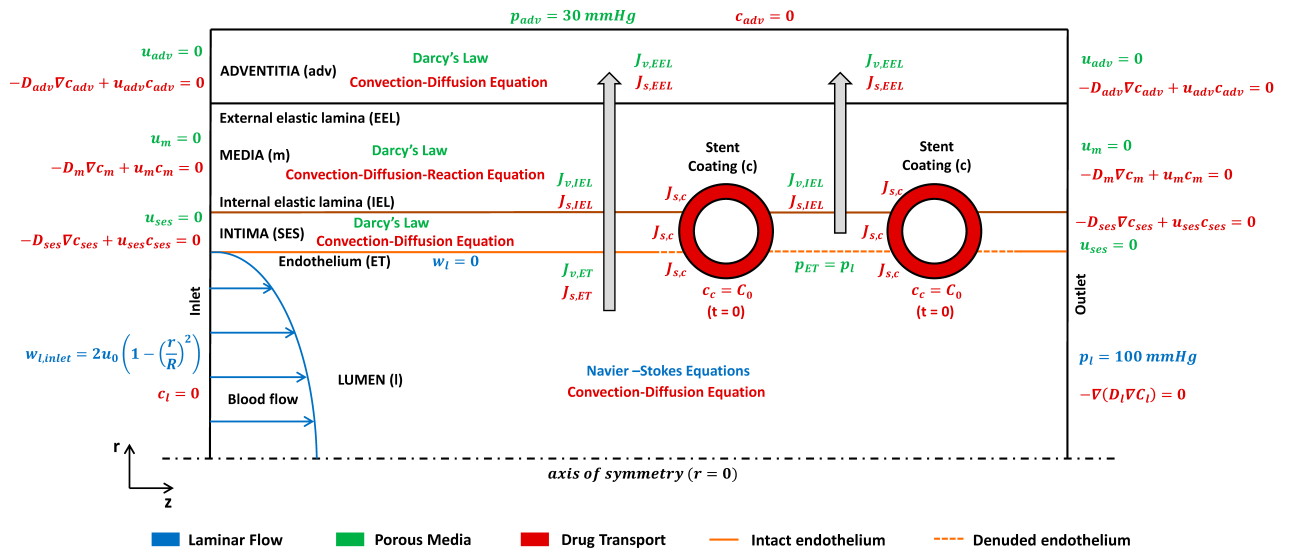


Fig. 2. Schematic showing boundary conditions of the drug transport model.

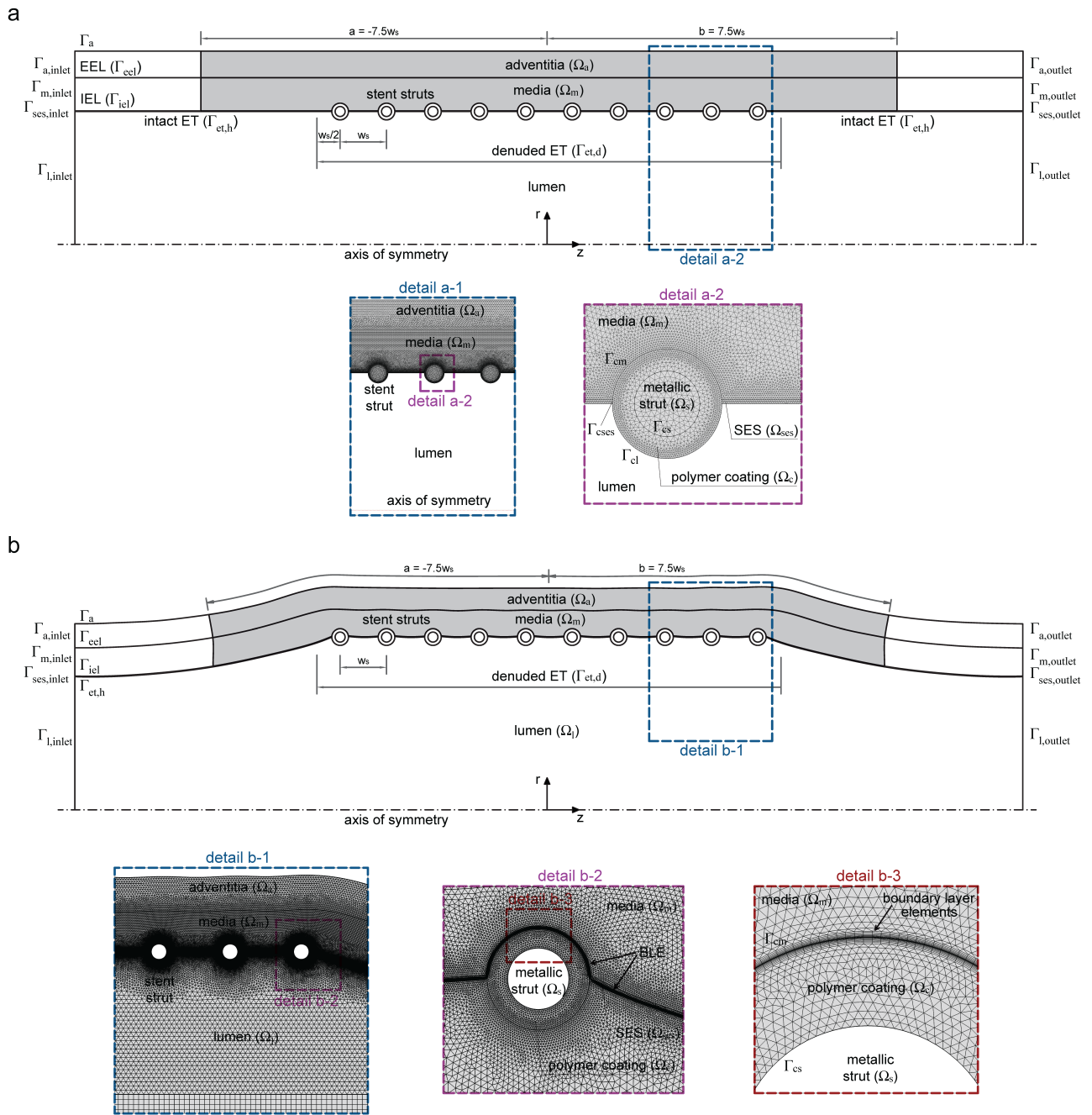


Fig. 3. The 3D arterial geometry is assumed to be axisymmetric and therefore a 2D representation is considered in this work. (a) Overall longitudinal section view of the pre-stressed arterial segment with a DES implanted. In details a-1 and a-2 a detailed view of the finite element (FE) mesh used in the mechanical model is shown. (b) Overall longitudinal section view of the arterial segment after stent deployment. In details b-1, b-2 and b-3 a detailed view of the FE mesh used in the drug transport analysis. In both subfigures, the therapeutic domain (target area for drug transport) considered to compute all the variables of the model is shaded in grey and it was defined as the domain that extends in  $a < z < b$  with the origin of the computational geometry placed between the two central struts and where  $a = -7.5w_s$  and  $b = 7.5w_s$ . In this figure,  $\Omega_l$  defines the vessel lumen,  $\Omega_{ses}$  the SES,  $\Omega_m$  the media,  $\Omega_a$  the adventitia,  $\Omega_s$  the metallic stent struts and  $\Omega_c$  the stent coating. The boundaries  $\Gamma_{et}$ ,  $\Gamma_{iel}$ ,  $\Gamma_{ecl}$  define the endothelium, internal and external elastic laminae, respectively;  $\Gamma_a$  the outer boundary of the arterial wall;  $\Gamma_{cl}$ ,  $\Gamma_{cses}$ ,  $\Gamma_{cm}$  and  $\Gamma_{cs}$  the interface between the stent coating and blood, SES, media and metallic strut, respectively;  $\Gamma_{l,inlet}$  and  $\Gamma_{l,outlet}$  the inlet and outlet boundaries of the lumen, respectively and;  $\Gamma_{i,inlet}$  and  $\Gamma_{i,outlet}$  the inlet and outlet boundaries of the wall layers with respect to the blood flow, respectively.

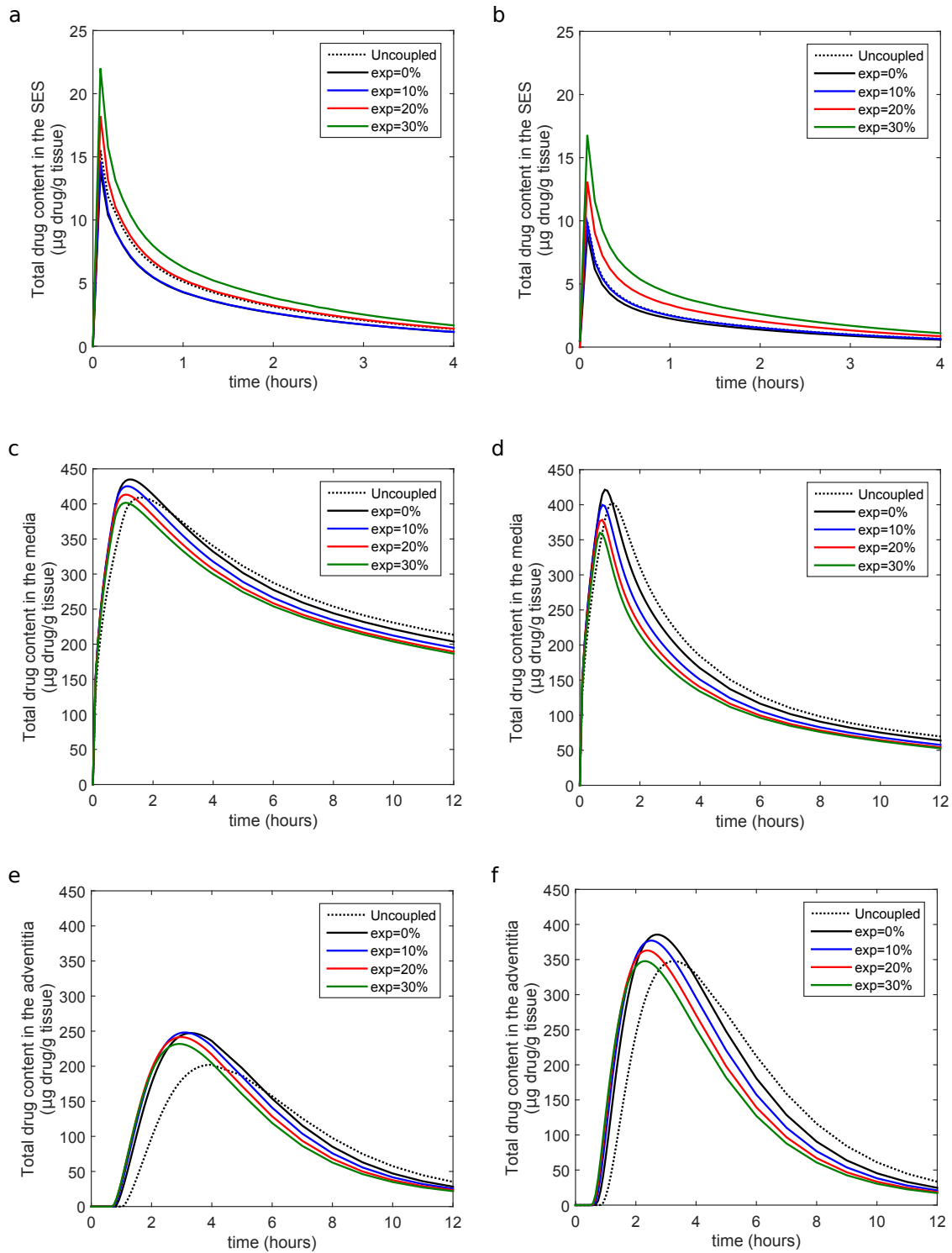


Fig. 4. Content of sirolimus (a, c, e) and paclitaxel (b, d, f) in each layer of the arterial wall (presented as  $\mu\text{g}$  drug per g of tissue). In the SES and the adventitia, drug content corresponds exclusively to free drug and in the media layer corresponds to free plus bound drug. Notice that the scales of the x- and y-axis in (a) and (b) are different from the rest of the subfigures. The results are shown for the uncoupled model and for luminal diameter expansions of 0 – 30% for the coupled model.

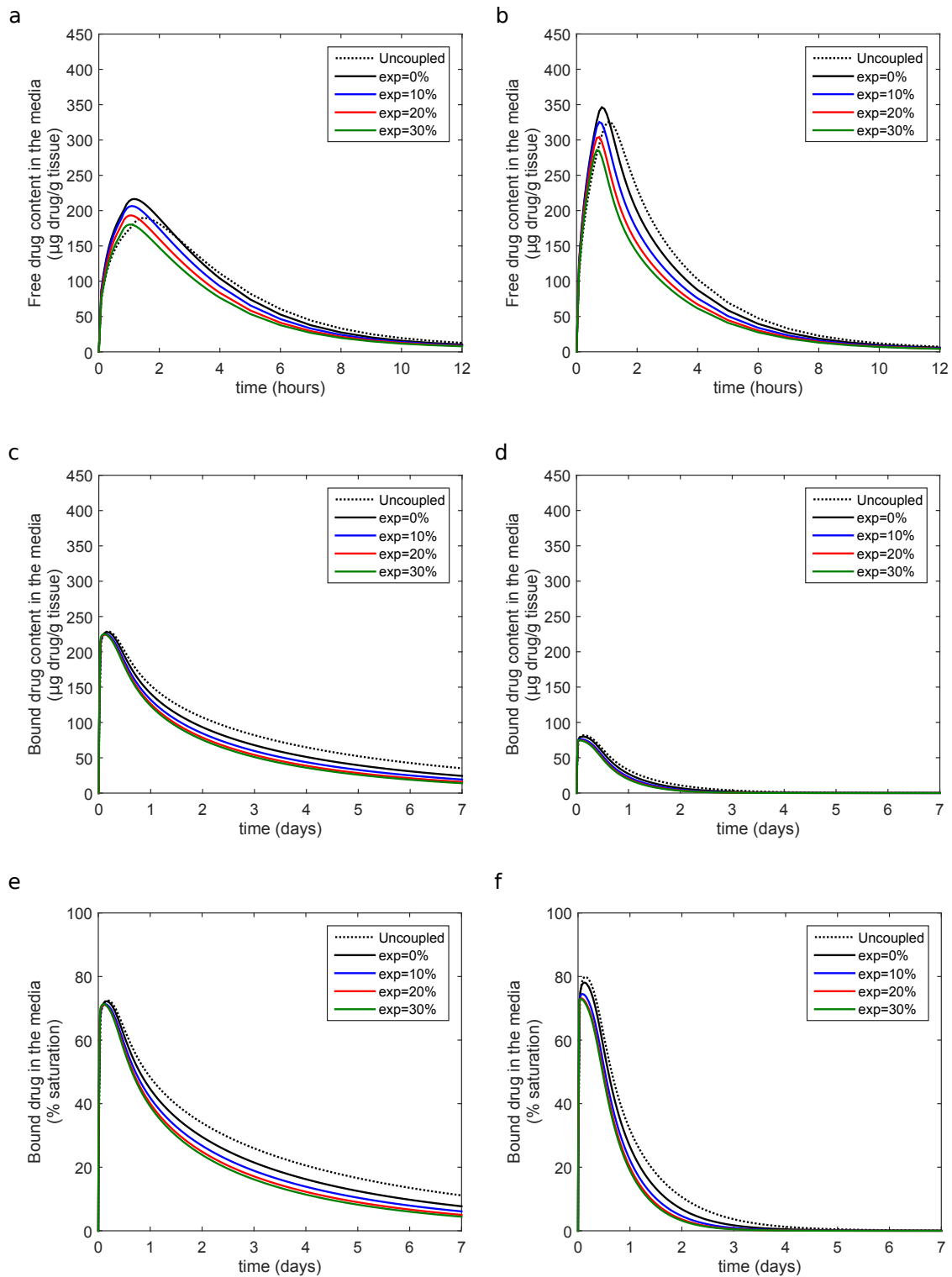


Fig. 5. Content of free sirolimus (a) and paclitaxel (b) in the media layer of the arterial wall (presented as  $\mu\text{g}$  drug per g of tissue). Content of bound of sirolimus (c) and paclitaxel (d) in the media (presented as  $\mu\text{g}$  drug per g of tissue). Binding site % saturation as a function of time for sirolimus (e) and paclitaxel (f) in the media. Note the different scales on the x- and y-axes. The results are shown for the uncoupled model and for luminal diameter expansions of 0 – 30% for the coupled model.

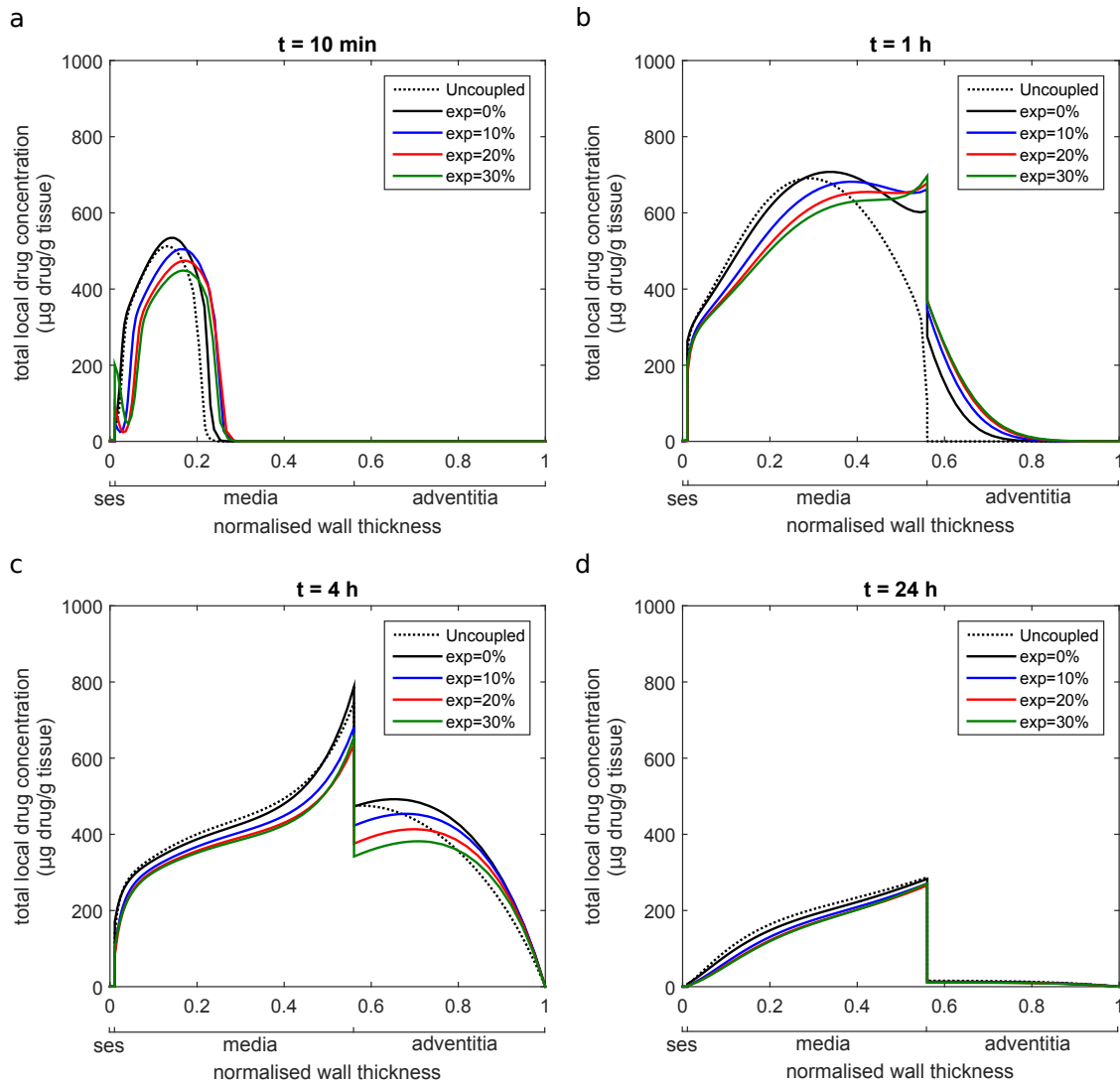


Fig. 6. Spatially varying profiles of total (free plus bound) local concentration of sirolimus in the tissue (presented as  $\mu\text{g drug per g of tissue}$ ) at 10 min (a), 1 hour (b), 4 hours (c) and 1 day (d) after stent implantation. The results are shown for the uncoupled model and for luminal diameter expansions of 0 – 30% for the coupled model in a radial section between the middle struts.

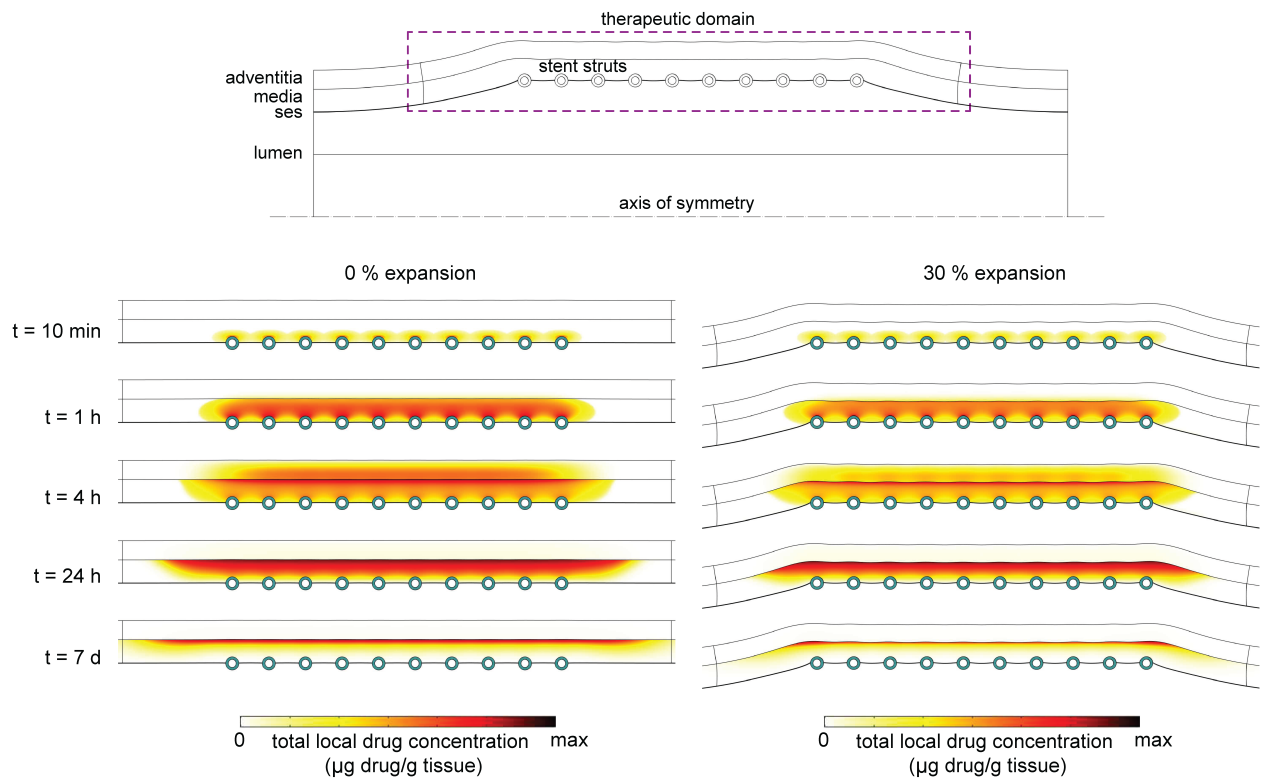


Fig. 7. Spatial variation of sirolimus at five different time points ( $t = 10 \text{ min}$ ,  $t = 1 \text{ hour}$ ,  $t = 4 \text{ hours}$ ,  $t = 24 \text{ hours}$  and  $t = 7 \text{ days}$ ) for the 0 % (left) and 30 % (right) expansion cases. For each time point the same colour scale is used for the 0 % and 30 % expansion cases. The maximum values of total local concentration of sirolimus chosen for each time point are presented as  $\mu\text{g drug/g tissue}$  and they are the following: at  $t = 10 \text{ min}$ ,  $\text{max} = 2722.67 \mu\text{g drug/g tissue}$ ; at  $t = 1 \text{ h}$ ,  $\text{max} = 1102.44 \mu\text{g drug/g tissue}$ ; at  $t = 4 \text{ h}$ ,  $\text{max} = 795.74 \mu\text{g drug/g tissue}$ ; at  $t = 24 \text{ h}$ ,  $\text{max} = 283.79 \mu\text{g drug/g tissue}$  and; at  $t = 7 \text{ d}$ ,  $\text{max} = 89.76 \mu\text{g drug/g tissue}$ . A comparison between spatial distribution in the tissue of sirolimus and paclitaxel for each expansion case and the corresponding tables with the maximum values at each time point may be found in the supplementary material.

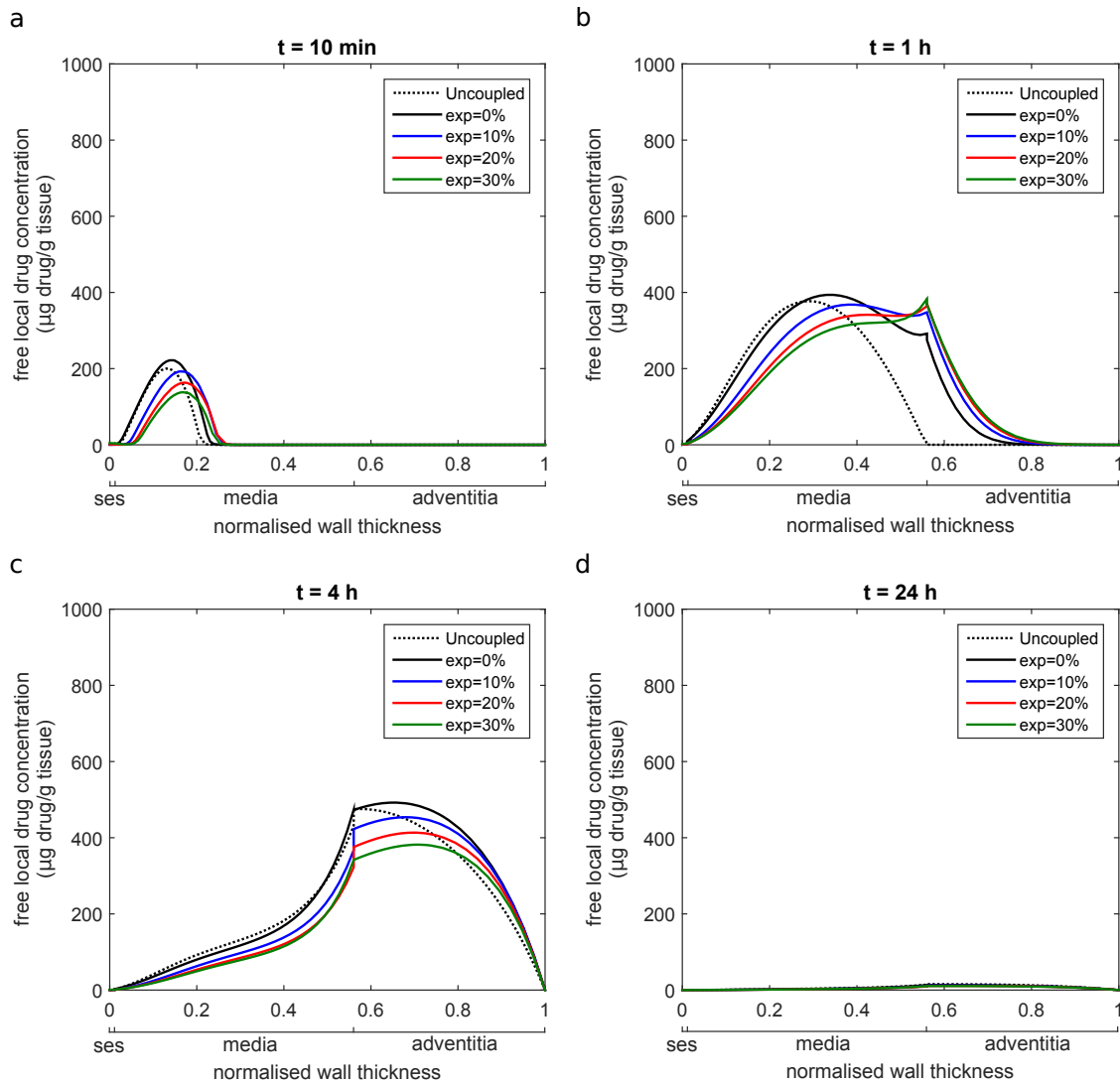


Fig. 8. Spatially varying profiles of free local concentration of sirolimus in the tissue (presented as  $\mu\text{g}$  drug per g of tissue) at 10 min (a), 1 hour (b), 4 hours (c) and 1 day (d) after stent implantation. The results are shown for the uncoupled model and for luminal diameter expansions of 0 – 30% for the coupled model in a radial section between the middle struts.

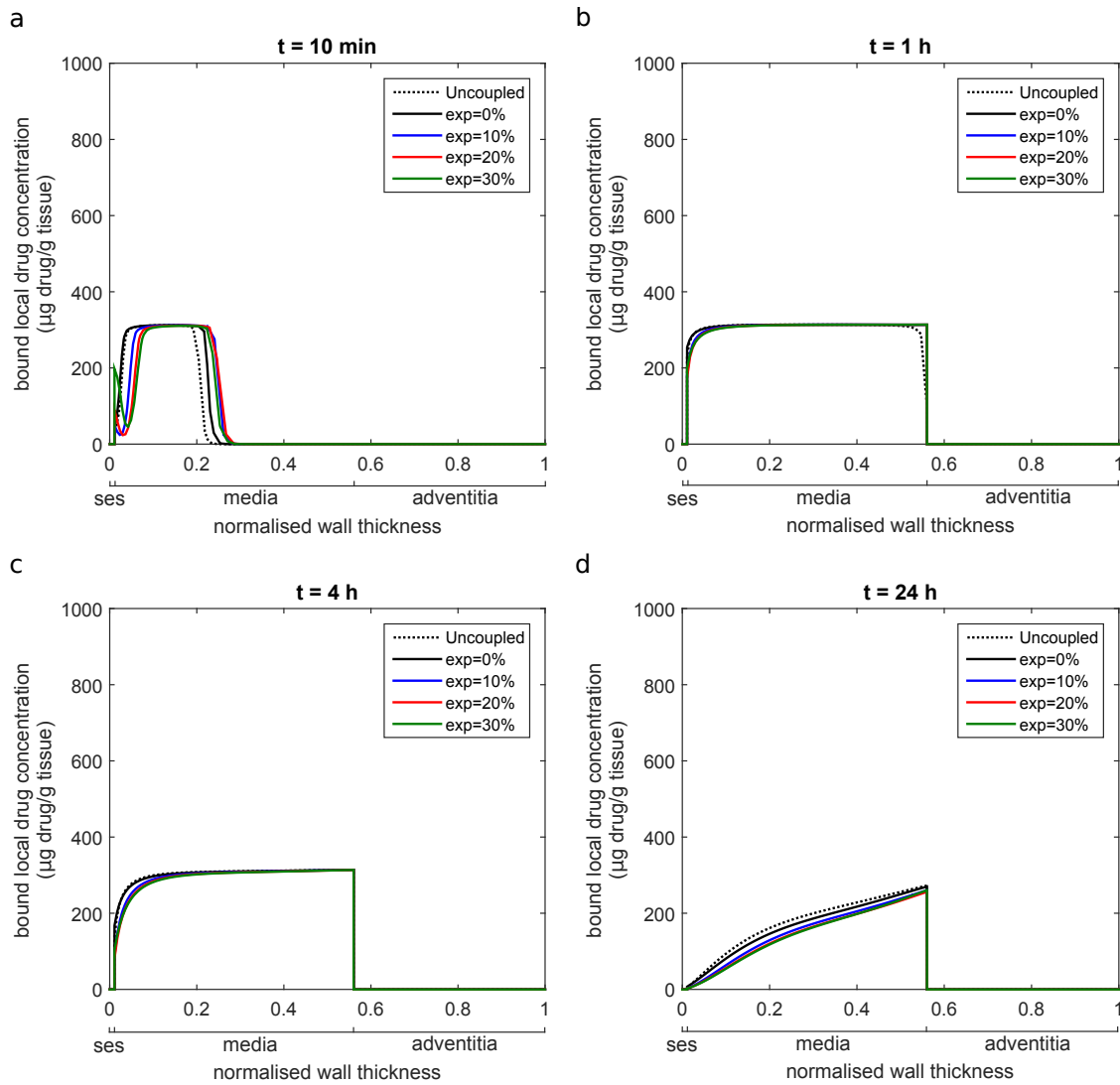


Fig. 9. Spatially varying profiles of local bound concentration of sirolimus in the tissue at 10 min (a), 1 hour (b), 4 hours (c) and 1 day (d) after stent implantation. The results are shown for the uncoupled model and for luminal diameter expansions of 0 – 30% for the coupled model in a radial section between the middle struts.

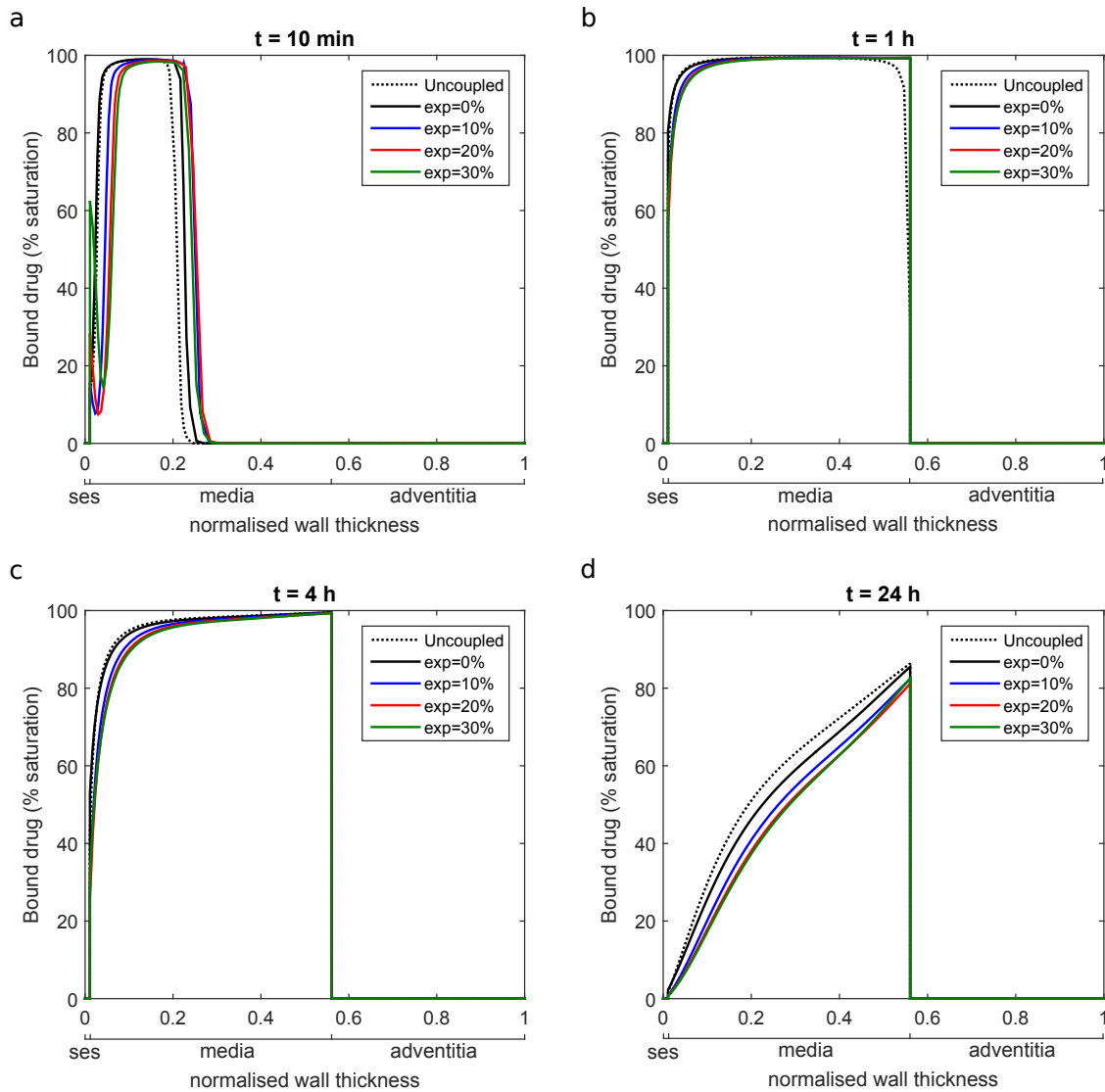


Fig. 10. Spatially varying profiles of binding site % saturation in the tissue at 10 min (a), 1 hour (b), 4 hours (c) and 1 day (d) after stent implantation, calculated as  $\frac{b_i}{b_{max}} \cdot 100$ . The results are shown for the uncoupled model and for luminal diameter expansions of 0 – 30% for the coupled model in a radial section between the middle struts.

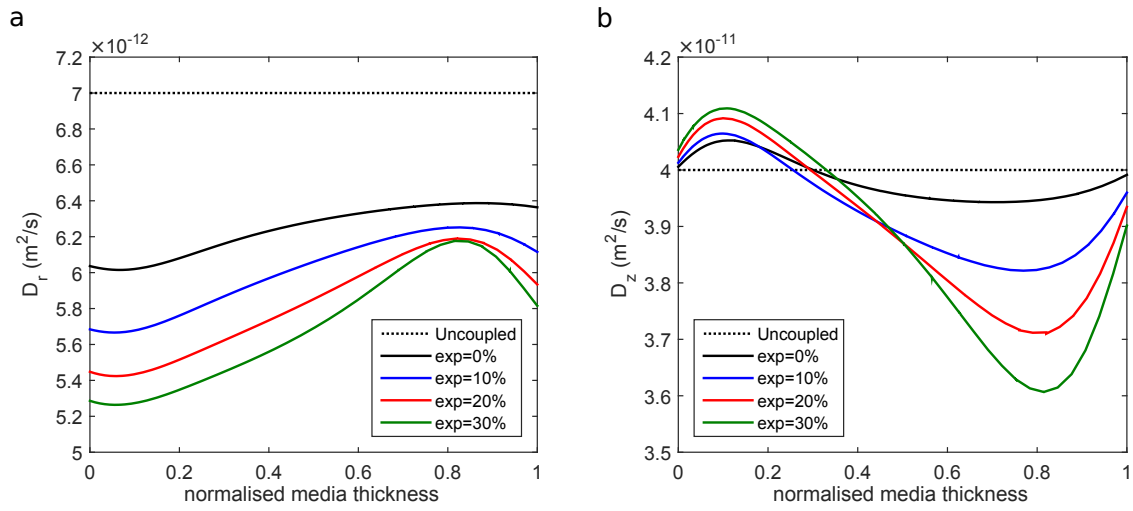


Fig. 11. Radial (a) and longitudinal (b) diffusion coefficients variation of sirolimus in the media layer of the arterial wall. The results are shown for the uncoupled model and for luminal diameter expansions of 0 – 30% for the coupled model. In both subfigures the radial line is drawn between the middle struts.

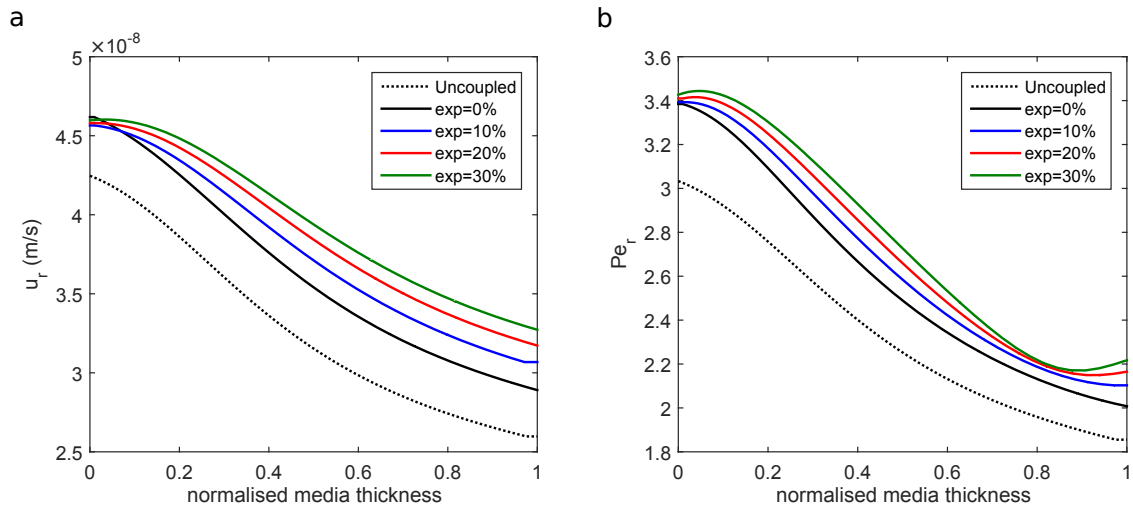


Fig. 12. (a) Radial component of flow in the media. (b) Radial Peclet number variation for sirolimus in the media layer of the arterial wall. The results are shown for the uncoupled model and for luminal diameter expansions of 0 – 30% for the coupled model. In both subfigures the radial line is drawn between the middle struts.